

Cosmological constraints on a decomposed Chaplygin gas

Yuting Wang^{1,2}, David Wands², Lixin Xu¹, Josue De-Santiago^{3,2} and Alireza Hojjati⁴

¹*School of Physics and Optoelectronic Technology, Dalian University of Technology,
Dalian, Liaoning 116024, People's Republic of China*

²*Institute of Cosmology & Gravitation, University of Portsmouth, Portsmouth, PO1 3FX, United Kingdom*

³*Universidad Nacional Autónoma de México, 04510, D. F., México*

⁴*Institute for the Early Universe, Ewha Womans University, Seoul, 120-750, South Korea*

(Dated: April 5, 2013)

Any unified dark matter cosmology can be decomposed into dark matter interacting with vacuum energy, without introducing any additional degrees of freedom. We present observational constraints on an interacting vacuum plus dark energy corresponding to a generalised Chaplygin gas cosmology. We consider two distinct models for the interaction leading to either a barotropic equation of state or dark matter that follows geodesics, corresponding to a rest-frame sound speed equal to the adiabatic sound speed or zero sound speed, respectively. For the barotropic model, the most stringent constraint on α comes from the combination of CMB+SNIa+LSS(m) gives $\alpha < 1.44 \times 10^{-5}$ at the 95% confidence level, which indicates that the barotropic model must be extremely close to the Λ CDM cosmology. For the case where the dark matter follows geodesics, perturbations have zero sound speed, and CMB+SNIa+gISW then gives the much weaker constraint $-0.1522 < \alpha < 0.2556$ at the 95% confidence level.

I. INTRODUCTION

The dominance of dark energy and dark matter in the present cosmological energy density has led many authors to seek a unified description in terms of a single dark component, referred to as unified dark matter or quartessence [1], which should explain both the current accelerated expansion of the universe and the role of non-baryonic dark matter in structure formation. One candidate from this kind of model, which has attracted a lot of attention, is the generalized Chaplygin gas (GCG) model [2]. It is a fluid, defined by an exotic equation of state:

$$P_{gCg} = -\frac{A}{\rho_{gCg}^\alpha}, \quad (1)$$

with model parameters α and A . The GCG model with $\alpha = 1$ reduces to the original Chaplygin gas model [3]. Predictions of the GCG cosmology has been tested against the different observational data, including type Ia supernovae [4–6], the positions of cosmic microwave background radiation peaks [7–9], the X-ray gas mass fraction of clusters [10], Hubble parameter-redshift data [11, 12], the lookback time-redshift data [13], gamma-ray bursts [14], and as well as various combinations of the updated data [15].

Going beyond constraints provided by the homogeneous background cosmology, the inclusion of inhomogeneous linear perturbations in the GCG has an effect on both the cosmic microwave background (CMB) anisotropies and structure formation. In particular, the imprint of a large integrated Sachs-Wolfe (ISW) signal [16], which arises from a time-dependent gravitational potential when dark energy dominates at late times in the Universe, could be observed on the CMB anisotropies [17, 18]. Recently, in [19] two of us revisited constraints on the GCG model from the combination of CMB, baryon acoustic oscillations (BAO), and type Ia supernovae (SNIa), including the full CMB temperature and polarization power spectra data. A tight bound for the parameter α was obtained up to the order of 10^{-3} .

The effect of the GCG on structure formation also contains important information. In [20], it was argued that in order to predict large-scale structure (LSS) consistent with the data from the 2dF survey [21], the GCG model has to be indistinguishable from Λ CDM, with $\alpha < \mathcal{O}(10^{-5})$. The slightly looser constraint, $\alpha < \mathcal{O}(10^{-4})$ was obtained in [22] by fitting the predicted baryon matter power spectrum, rather than the total matter power spectrum, to the Sloan Digital Sky Survey (SDSS) DR7 power spectrum data. In either case a stringent limit on the α parameter is required from the LSS power spectrum data because there are instabilities or oscillations of GCG power spectra due to the adiabatic pressure perturbation produced for non-zero α . This problem can be avoided in some unified dark matter models by requiring a fast transition between a CDM-like era and a Λ CDM-like phase [23, 24].

In order to save the GCG model some type of intrinsic entropy perturbation must be introduced in the GCG fluid to counteract the effect caused by the adiabatic GCG pressure perturbation, as in the so-called silent GCG model [25]. The combined constraints from data on both the silent GCG and standard GCG model are presented in [26]. It is shown that with a vanishing GCG pressure perturbation there is a much wider allowed parameter range, $-0.3 < \alpha < 0.7$ [26]. Subsequently, the ISW data [27] was used to constrain the silent GCG model [28]. The required entropy perturbation can be introduced by decomposing the GCG fluid into two components of dark matter and dark energy [29], but the possible ways of decomposition are not unique. In [30] the GCG model was split into dark matter and vacuum energy, considering a homogeneous vacuum when studying density perturbations in the Newtonian limit.

Recently it has been shown that any unified dark matter model can be decomposed into dark matter interacting with a vacuum energy (with equation of state $P = -\rho$) without introducing any additional degrees of freedom [31]. In general an interacting vacuum energy is inhomogenous, and a description of the dynamics of inhomogeneous vacuum energy was presented in [31, 32].

In this paper we will study in detail the constraints on a decomposed GCG model described by dark matter interacting with inhomogeneous vacuum energy. A closed set of perturbation equations are obtained once a covariant form is specified for the interaction. Firstly, we consider a model in which the vacuum energy is a function of the local matter density. We show this leads to a barotropic equation of state for the dark matter+vacuum, and hence reproduces previous results for a unified GCG. Secondly we consider an energy-momentum transfer parallel to the matter four-velocity, leading to a geodesic flow for the matter. In both cases we consider background cosmologies that mimic the GCG cosmologies, but the evolution of linear perturbations differs due to the presence of non-adiabatic pressure perturbations. We pay particular attention to their imprints on the CMB and LSS power spectra. To constrain the barotropic and geodesic model parameters we will use different combinations of current cosmological data including the CMB temperature and polarization power spectra [33], SNIa from the Union2.1 compilation of the Supernova Cosmology Project Collaboration [34], the BAO distance measurements [35], the LSS power spectrum from SDSS DR7 [36], and the galaxy-ISW (gISW) cross-correlation power spectra from [37].

This paper is organized as follows. In the next section, we review the background equations for the GCG model. In Sec. III, the linear perturbation equations for both the unified GCG model and the two decomposed models are presented. In Sec. IV, we show the effects on CMB and LSS power spectra in the two decomposed models, then perform a global fitting to observational data by using the MCMC method and discuss the resulting constraints on the interaction. In the final section we present our conclusions. In what follows (unless otherwise specified) the illustrative plots are shown using the joint mean values for cosmological parameters from WMAP7 data [33]: $\Omega_b h^2 = 0.02255$, $\Omega_{dm} h^2 = 0.1126$, $h = 0.702$, $\tau = 0.088$, $n_s = 0.968$, and $A_s = 2.43 \times 10^{-9}$ at $k_{s0} = 0.002 \text{Mpc}^{-1}$.

II. CHAPLYGIN GAS COSMOLOGY

We will consider a spatially-flat, homogeneous and isotropic Friedmann-Robertson-Walker universe with metric

$$ds^2 = -dt^2 + a^2(t)\delta_{ij}dx^i dx^j , \quad (2)$$

where the Friedmann equation is given by

$$H^2 \equiv \left(\frac{\dot{a}}{a}\right)^2 = \frac{8\pi G}{3}(\rho_b + \rho_r + \rho_{gCg}) , \quad (3)$$

where ρ_b , ρ_r and ρ_{gCg} are the energy densities of baryons, radiation and a generalised Chaplygin gas (GCG) which can act as both a dark energy component, accelerating the universe at late times, and dark matter. The energy conservation equations for the various components read

$$\dot{\rho}_b + 3H\rho_b = 0 , \quad (4)$$

$$\dot{\rho}_r + 4H\rho_r = 0 , \quad (5)$$

$$\dot{\rho}_{gCg} + 3H(\rho_{gCg} + P_{gCg}) = 0 . \quad (6)$$

The equation of state for GCG (1) then allows us to integrate Eq. (6) to obtain

$$\rho_{gCg} = \rho_{gCg0} \left[B_s + (1 - B_s)a^{-3(1+\alpha)} \right]^{1/(1+\alpha)} , \quad (7)$$

where ρ_{gCg0} is present value of energy density of GCG (when $a = a_0 = 1$) and we have replaced A in Eq. (1) with the dimensionless model parameter, $B_s = A/\rho_{gCg0}^{1+\alpha}$.

In a previous work we have shown that a unified dark matter fluid with an arbitrary equation of state can be decomposed into pressureless dark matter interacting with a vacuum energy, V , with an appropriate energy transfer [31]. For the GCG solution (7), we can write

$$\rho_{gCg} = \rho_{dm} + V , \quad (8)$$

such that, from Eq. (1)

$$A = V(\rho_{dm} + V)^\alpha . \quad (9)$$

The conservation equations of dark matter and vacuum energy are

$$\dot{\rho}_{dm} + 3H\rho_{dm} = -Q, \quad (10)$$

$$\dot{V} = Q. \quad (11)$$

Thus from Eqs. (9), (10) and (11), we obtain

$$Q = 3\alpha H \frac{\rho_{dm} V}{\rho_{dm} + V}. \quad (12)$$

In the decomposed model (8), the parameter, B_s in Eq. (7), can be written in terms of the present values of the energy densities, $B_s = [V/(\rho_{dm} + V)]_0$. The decomposed model is characterised by a single dimensionless parameter α [31], but an FRW solution is specified by two boundary conditions (such as the present density of matter and vacuum) whereas the original GCG model is specified by two model parameters, α and A (or B_s) and one boundary condition. This already suggests that the decomposed model may naturally accommodate non-adiabatic density perturbations, in addition to the adiabatic perturbations of the original GCG. As we shall see, this can have important consequences for the evolution of perturbations in a decomposed model.

Note that the Friedmann equation (3) can be written as

$$H^2 = H_0^2 \left\{ \Omega_b a^{-3} + \Omega_r a^{-4} + (\Omega_V + \Omega_{dm}) \left[\frac{\Omega_V}{\Omega_V + \Omega_{dm}} + \frac{\Omega_{dm}}{\Omega_V + \Omega_{dm}} a^{-3(1+\alpha)} \right]^{\frac{1}{1+\alpha}} \right\}, \quad (13)$$

where the dimensionless fractional energy density of individual components is defined as

$$\Omega_I = \left(\frac{8\pi G \rho_I}{3H^2} \right)_0, \quad (14)$$

which satisfies $\Omega_b + \Omega_r + \Omega_V + \Omega_{dm} = 1$.

We illustrate the background evolution as a function of redshift for different values of the parameter α in Fig. 1. In the particular case when $\alpha = 0$, the background evolution is identical to that for the Λ CDM model.

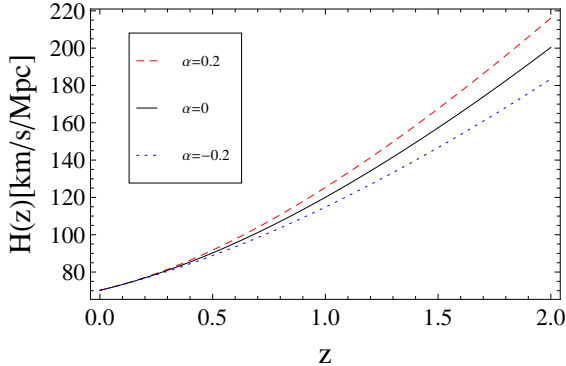


FIG. 1: The Hubble parameter as a function of redshift z for different values of parameter α , where the black line with $\alpha = 0$ corresponds to Λ CDM model.

III. THE LINEAR PERTURBATION EQUATIONS

We begin with a general scalar mode of the metric perturbation in an arbitrary gauge with the perturbed line of element [38–41]

$$ds^2 = -(1 + 2\phi)dt^2 + 2a\partial_i B dt dx^i + a^2 [(1 - 2\psi)\delta_{ij} + 2\partial_i \partial_j E] dx^i dx^j. \quad (15)$$

The Einstein equations are [38–41]

$$3H(\dot{\psi} + H\phi) - \frac{\nabla^2}{a^2}(\psi + H\sigma) = -4\pi G\delta\rho, \quad (16)$$

$$\dot{\psi} + H\phi = -4\pi G(\rho + P)\theta, \quad (17)$$

$$\dot{\sigma} + H\sigma - \phi + \psi = 8\pi G\Pi, \quad (18)$$

$$\ddot{\psi} + 3H\dot{\psi} + H\dot{\phi} + (3H^2 + 2\dot{H})\phi = 4\pi G \left(\delta P + \frac{2}{3} \frac{\nabla^2}{a^2} \Pi \right), \quad (19)$$

where $\sigma \equiv a^2 \dot{E} - aB$ is the shear, $\delta\rho$ is the total density perturbation, δP is the total pressure perturbation, Π is the total anisotropic stress, and θ is the total covariant velocity perturbation¹.

For each individual component, the covariant conservation equation allowing for energy-momentum transfer gives

$$\nabla_\mu T_{(I)}^{\mu\nu} = Q_{(I)}^\nu. \quad (20)$$

General relativity requires conservation of the total energy-momentum, $\nabla_\mu T^{\mu\nu} = 0$, so we have $\sum_I Q_{(I)}^\nu = 0$. The perturbed energy-momentum transfer four-vector is conventionally split into the energy transfer, $Q_I + \delta Q_I$, and momentum transfer, f_I , relative to the total four-velocity [40–43]

$$Q_\mu^{(I)} = [-Q_I(1 + \phi) - \delta Q_I, \partial_i(f_I + Q_I\theta)]. \quad (21)$$

The energy and momentum conservation equations for each fluid component are then [39–41, 43]:

$$\dot{\rho}_I + 3H(\delta\rho_I + \delta P_I) - 3(\rho_I + P_I)\dot{\psi} + (\rho_I + P_I)\frac{\nabla^2}{a^2}(\theta_I + \sigma) = \delta Q_I + Q_I\phi, \quad (22)$$

$$(\rho_I + P_I)\dot{\theta}_I - 3c_{sI}^2 H(\rho_I + P_I)\theta_I + (\rho_I + P_I)\phi + \delta P_I + \frac{2}{3}\frac{\nabla^2}{a^2}\Pi_I = f_I + Q_I\theta - (1 + c_{sI}^2)Q_I\theta_I, \quad (23)$$

where $c_{sI}^2 = \dot{P}_I/\dot{\rho}_I$ is the adiabatic sound speed.

The numerical code CAMB [44] is written in the synchronous gauge, so in order to place quantitative constraints on the model parameters we will solve the equations in a synchronous gauge [45] where

$$\phi = B = 0, \quad \psi = \eta, \quad \text{and} \quad k^2 E = -\frac{h}{2} - 3\eta. \quad (24)$$

There is a residual spatial gauge freedom in the synchronous gauge which allows one to set the initial velocity of any component to zero. We see from Eq. (23) that it is possible to work in a gauge in which $\theta_I = 0$ at all times for non-interacting, pressureless matter. A comoving synchronous gauge is commonly used, in which the dark matter velocity is zero, $\theta_{dm} = 0$. This is no longer possible in models where the dark matter experiences a momentum transfer, $f_{dm} + Q_{dm}(\theta - \theta_{dm}) \neq 0$. We can still work in a synchronous gauge, but note that the dark matter velocity is not necessarily zero.

The time-time and time-space components of the perturbed Einstein field equations, (16) and (17), in the synchronous gauge are

$$\frac{\dot{h}}{2} = \frac{1}{H} \left(\frac{k^2}{a^2} \eta + 4\pi G \delta\rho \right), \quad (25)$$

$$\dot{\eta} = -4\pi G(\rho + P)\theta. \quad (26)$$

Together with the energy and momentum conservation equations for each component, these form a closed set of equations.

After decoupling, the baryon component is conserved independently and the perturbation equations for the baryon density contrast and velocity are given by

$$\dot{\delta}_b - \frac{k^2}{a^2}\theta_b = -\frac{\dot{h}}{2}, \quad (27)$$

$$\dot{\theta}_b = 0. \quad (28)$$

Combining Eqs. (18), (19) in the synchronous gauge and Eq. (25), we have

$$\ddot{h} + 2H\dot{h} = -8\pi G(\delta\rho + 3\delta P). \quad (29)$$

By differentiating Eq. (27) with respect to time and combining Eq. (28) and the above equation, we find a second-order differential equation for the baryonic density contrast

$$\ddot{\delta}_b + 2H\dot{\delta}_b = 4\pi G(\delta\rho + 3\delta P). \quad (30)$$

¹ Note that $\theta \equiv a(v + B)$ in terms of the total velocity potential v defined in, e.g., Ref. [41].

A. Unified GCG model

In the unified GCG model, the energy-momentum tensor of the GCG is conserved and hence Eqs. (22) and (23) give the perturbed energy and momentum conservation equations

$$\dot{\delta}_{gCg} + 3H(c_{s,gCg}^2 - w_{gCg})\delta_{gCg} + (1 + w_{gCg})\left(-\frac{k^2}{a^2}\theta_{gCg} + \frac{\dot{h}}{2}\right) = 0, \quad (31)$$

$$\dot{\theta}_{gCg} - 3c_{s,gCg}^2 H\theta_{gCg} + \frac{c_{s,gCg}^2}{1 + w_{gCg}}\delta_{gCg} = 0, \quad (32)$$

where the adiabatic sound speed for the GCG is fixed by the equation of state of the GCG

$$c_{s,gCg}^2 = -\alpha w_{gCg}, \quad (33)$$

$$w_{gCg} = -\frac{B_s}{B_s + (1 - B_s)a^{-3(1+\alpha)}}. \quad (34)$$

We can derive a second-order differential equation for GCG overdensity by differentiating Eq. (31) with respect to time and combining Eqs. (29) and (32):

$$\begin{aligned} \ddot{\delta}_{gCg} &+ 2H[1 + 3(c_{s,gCg}^2 - w_{gCg})]\dot{\delta}_{gCg} \\ &+ [3\dot{H}(c_{s,gCg}^2 - w_{gCg}) + 3H(c_{s,gCg}^2 - w_{gCg}) + 9H^2(c_{s,gCg}^2 - w_{gCg})^2 + 6H^2(c_{s,gCg}^2 - w_{gCg})]\delta_{gCg} \\ &= -c_{s,gCg}^2 \frac{k^2}{a^2} \delta_{gCg} + (1 + w_{gCg})3c_{s,gCg}^2 H \frac{k^2}{a^2} \theta_{gCg} + (1 + w_{gCg})4\pi G(\delta\rho + 3\delta P). \end{aligned} \quad (35)$$

The first term on the right-hand-side of the above equation dominates in the small-scale limit and the adiabatic pressure perturbation causes the instabilities (or oscillations) of density perturbations for negative (or positive) α [46].

B. Interacting vacuum energy + dark matter models

In an interacting vacuum energy + dark matter model, the energy continuity equations (22) for the dark matter and vacuum energy in the synchronous gauge become

$$\dot{\delta\rho}_{dm} + 3H\delta\rho_{dm} + \rho_{dm}\left(-\frac{k^2}{a^2}\theta_{dm} + \frac{\dot{h}}{2}\right) = \delta Q_{dm}, \quad (36)$$

$$\dot{\delta V} = \delta Q_V, \quad (37)$$

while the momentum conservation equations (23) are given by

$$\rho_{dm}\dot{\theta}_{dm} = f_{dm} + Q_{dm}(\theta - \theta_{dm}), \quad (38)$$

$$-\delta V = f_V + Q_V\theta. \quad (39)$$

Note that the vacuum energy has vanishing momentum and therefore the force exerted on the vacuum, $\partial_i(f_V + Q_V\theta)$, is exactly cancelled by the gradient of the vacuum pressure, $\partial_i(-\delta V)$.

The conservation of total energy-momentum for the interacting dark matter and vacuum energy implies that

$$Q_V = -Q_{dm} = Q, \quad \delta Q_V = -\delta Q_{dm}, \quad f_V = -f_{dm}. \quad (40)$$

We can then eliminate δQ_{dm} and f_{dm} using the energy and momentum conservation equations for the vacuum (37) and (39) to leave the energy-momentum conservation equations for the dark matter

$$\dot{\delta}_{dm} - \frac{Q}{\rho_{dm}}\delta_{dm} - \frac{k^2}{a^2}\theta_{dm} + \frac{\dot{h}}{2} = -\frac{\dot{\delta V}}{\rho_{dm}} \quad (41)$$

$$\rho_{dm}\dot{\theta}_{dm} = \delta V + Q\theta_{dm}, \quad (42)$$

where the background energy transfer Q is given by Eq. (12). We now need to specify the form of the vacuum interaction to determine the vacuum perturbation, δV , and obtain a closed set of equations.

1. Barotropic model

Firstly, we consider a model in which the vacuum energy density is a function of local dark matter density

$$V = V(\rho_{dm}). \quad (43)$$

This implies that the energy transfer between the vacuum and the dark matter is along the gradient of the local dark matter density: $Q_V^\mu \propto \nabla^\mu \rho_{dm}$.

At linear order, we have

$$\delta V = \frac{\dot{V}}{\dot{\rho}_{dm}} \delta \rho_{dm}, \quad (44)$$

which shows that in this case the relative perturbations between the vacuum and the dark matter are adiabatic. The total pressure perturbation for the interacting dark matter+vacuum energy is

$$\begin{aligned} -\delta V &= \frac{\alpha V}{\rho_{dm} + V} (\delta \rho_{dm} + \delta V) \\ &= c_{s,gCg}^2 (\delta \rho_{dm} + \delta V). \end{aligned} \quad (45)$$

Therefore, the sound speed for the interacting dark matter+vacuum energy is exactly the same as the adiabatic sound speed for the original generalised Chaplygin gas, $c_{s,gCg}^2$ given by Eq. (33) [31, 32]. We show the effect on the sound speed caused by the parameter α in Fig. 2.

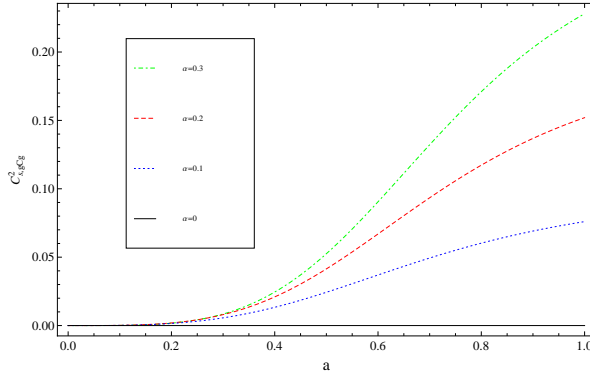


FIG. 2: The sound speed as a function of scale factor a for the barotropic model.

In the synchronous gauge, we have from Eqs. (41), (42) and (44)

$$\dot{\delta}_{dm} = \frac{(1+\alpha)Q}{\rho_{dm} + (1+\alpha)V} \delta_{dm} + \frac{\rho_{dm} + (1+\alpha)V}{\rho_{dm} + V} \frac{k^2}{a^2} \theta_{dm} - \frac{\rho_{dm} + (1+\alpha)V}{\rho_{dm} + V} \frac{\dot{h}}{2}, \quad (46)$$

$$\dot{\theta}_{dm} = \frac{Q}{\rho_{dm}} \theta_{dm} - \frac{\alpha V}{\rho_{dm} + (1+\alpha)V} \delta_{dm}, \quad (47)$$

It is clear that the barotropic model with $\alpha = 0$ reduces to the Λ CDM model at the linear order. Comparing with dark matter perturbations in the standard Λ CDM model, we can see that density contrasts and velocities of the interacting dark matter evolve very differently. In this case, due to the presence of momentum transfer, θ_{dm} will evolve to be nonzero, even if its initial value is set to zero. Therefore, the synchronous gauge is not comoving with the interacting dark matter and we calculate the perturbed equations in an arbitrary synchronous gauge [47].

Combining Eqs. (46) and (47) with Eq. (29), we obtain a second-order differential equation for the dark matter overdensity

$$\begin{aligned} \ddot{\delta}_{dm} &- \left[\frac{2(1+\alpha)Q}{\rho_{dm} + (1+\alpha)V} - 2H \right] \dot{\delta}_{dm} \\ &- \left\{ \left[\frac{(1+\alpha)Q}{\rho_{dm} + (1+\alpha)V} \right] \dot{\theta}_{dm} - \left[\frac{(1+\alpha)Q}{\rho_{dm} + (1+\alpha)V} \right]^2 + 2H \left[\frac{(1+\alpha)Q}{\rho_{dm} + (1+\alpha)V} \right] \right\} \delta_{dm} \\ &= -c_{s,gCg}^2 \frac{k^2}{a^2} \delta_{dm} + \left(1 + \frac{\alpha V}{\rho_{dm} + V} \right) \frac{Q}{\rho_{dm}} \frac{k^2}{a^2} \theta_{dm} + \left(1 + \frac{\alpha V}{\rho_{dm} + V} \right) 4\pi G(\delta\rho + 3\delta P). \end{aligned} \quad (48)$$

The first term on the right-hand-side of Eq. (48) dominates in the small-scale limit. Negative α causes instabilities of density perturbations. Conversely, there are oscillations of perturbations for positive α . In order to avoid the presence of negative sound speed, we will require $\alpha \geq 0$ in this case.

We find that the perturbations for the barotropic model, Eqs. (46), (47) and (48), obey the same dynamical evolutions as those for the unified GCG model, Eqs. (31), (32) and (35), where we identify

$$\delta_{gCg} = \frac{\rho_{dm}}{\rho_{dm} + (1 + \alpha)V} \delta_{dm}, \quad \theta_{gCg} = \theta_{dm}. \quad (49)$$

We should not be surprised that this interacting model reproduces the same behaviour as the GCG since by requiring $V = V(\rho_{dm})$ we have set the pressure of the interacting matter+vacuum $P_{dm+V} = -V$ to be an implicit function of $\rho_{dm} + V$, i.e., we have a barotropic fluid.

The evolution of the dark matter density perturbations for the barotropic model on a fixed scale is shown in Fig. 3. On the left panel, it is shown that increasing α causes the suppression of the growth of density fluctuations on the scale, $k = 0.001[\text{h Mpc}^{-1}]$. For the smaller scale, $k = 0.01[\text{h Mpc}^{-1}]$, on the right panel, we can see that density fluctuations rapidly decay and oscillate with increasing α .

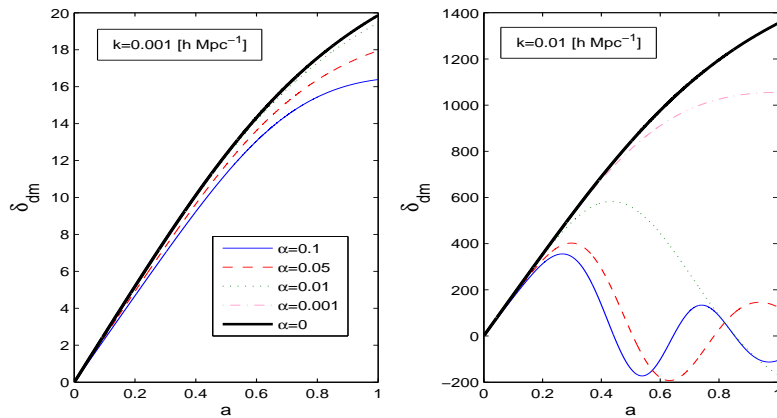


FIG. 3: The dark matter density perturbations on fixed scales: $k = 0.001 [\text{h Mpc}^{-1}]$ (left panel) and $k = 0.01 [\text{h Mpc}^{-1}]$ (right panel) as a function of scale factor for the barotropic model. The blue line, red line, green line, pink line and black line correspond to $\alpha = 0.1, 0.05, 0.01, 0.001, 0$ (ΛCDM model), respectively.

2. Geodesic model

An alternative model for the energy transfer is to consider an energy flow that is parallel to the 4-velocity of the dark matter:

$$Q_{(dm)}^\mu = -Qu_{(dm)}^\mu. \quad (50)$$

For this form of the covariant interaction there is no momentum transfer in the rest frame of dark matter [48, 49], $f_{dm} - Q(\theta - \theta_{dm}) = 0$ in Eq. (21). The velocity perturbation for dark matter is not affected by the interaction and obeys the standard equation, $\dot{\theta}_{dm} = 0$ from Eq. (38). This allows us to work in a synchronous gauge that is comoving with the dark matter ($\theta_{dm} = 0$). The dark matter 4-velocity, u^μ is thus a geodesic flow: $u_{(dm)}^\mu \nabla_\mu u_{(dm)}^\nu = 0$. Hence we will refer to this form of energy-transfer as a geodesic model.

The vacuum perturbation in the dark matter-comoving frame is identically zero, from Eq. (42),

$$\delta V_{com} = \delta V + \dot{V}\theta_{dm} = 0. \quad (51)$$

The pressure perturbation for the interacting vacuum+dark matter is therefore zero in the dark matter rest frame and thus the speed of sound for the interacting vacuum+dark matter is zero [31, 32]. Note that this implies that in this case there is a non-adiabatic pressure perturbation, due to the relative entropy perturbation between the dark matter and the vacuum energy [31, 32], in contrast to the barotropic model.

From Eq. (41), the perturbation equation for the dark matter density contrast in the rest frame of dark matter obeys

$$\dot{\delta}_{dm} = -\frac{\dot{h}}{2} + \frac{Q}{\rho_{dm}} \delta_{dm}. \quad (52)$$

We see that, again, the case with $\alpha = 0$ is completely equivalent to Λ CDM at linear order.

A second-order differential equation for the dark matter overdensity can be derived from the above equation and Eq. (29), which gives

$$\ddot{\delta}_{dm} + \left(-\frac{Q}{\rho_{dm}} + 2H \right) \dot{\delta}_{dm} - \left[2H \frac{Q}{\rho_{dm}} + \left(\frac{\dot{Q}}{\rho_{dm}} \right) \right] \delta_{dm} = 4\pi G(\delta\rho + 3\delta P). \quad (53)$$

We plot the evolution of the dark matter density perturbations on different scales in Fig. 4. Compared with the growth in the Λ CDM model, positive α indicates that there is an energy transfer from dark matter to vacuum energy, so the growth of density perturbations with positive α is suppressed at early times during matter-domination. At late times, vacuum energy dominates in the universe, and the vacuum interaction drives the growth of dark matter density perturbations. Conversely, for the negative α the growth of density perturbations is enhanced at early times and is gradually suppressed at late times. Note that there is no instability associated with imaginary speed of sound for $\alpha < 0$ in the geodesic model.

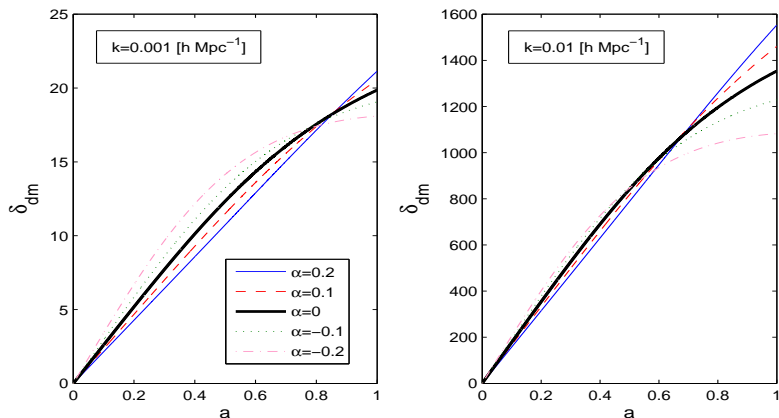


FIG. 4: The dark matter density perturbations on fixed scales: $k = 0.001 [\text{h Mpc}^{-1}]$ (left panel) and $k = 0.01 [\text{h Mpc}^{-1}]$ (right panel) as a function of scale factor for the geodesic model. The blue line, red line, black line, green line and pink line correspond to $\alpha = 0.2, 0.1, 0$ (Λ CDM model), $-0.1, -0.2$, respectively.

IV. COSMOLOGICAL CONSTRAINTS

A. Theoretical predictions of CMB and LSS power spectra

First, we illustrate the imprint on the CMB and LSS power spectra for different values of the parameter α for both the barotropic model and geodesic model. For the barotropic model we will restrict the value of α to be greater than or equal to zero in order to avoid instabilities due to an imaginary sound speed, but we will extend α to negative values for the geodesic model since the sound speed remains real in that case.

The effects on the CMB power spectra are shown in Fig. 5. From the left panel, positive α leads to an energy transfer from dark matter to vacuum energy. Increasing α causes the matter-radiation equality to happen earlier and hence suppresses the first acoustic peaks. Conversely, negative α delays the epoch of matter-radiation equality, and hence amplifies the acoustic peaks, as shown in the geodesic case on the right panel of Fig. 5.

One source of CMB anisotropies at low multipoles is the ISW effect. The amplitude of the ISW signal on large scales is affected not only by the epoch of dark matter-vacuum energy equality, but is also modified directly by the evolution of the gravitational potential, which differs in the barotropic and geodesic models. These two competing mechanisms give the final ISW signal.

In order to clearly express the ISW effect caused by the time-varying gravitational potential, we calculate the Newtonian potential, ψ^N , corresponding to the metric perturbation, ψ , in the Newtonian or longitudinal gauge ($B = E = 0$) [45].

This is given by the relativistic Poisson equation [40]

$$k^2 \psi^N = -4\pi G a^2 \rho \Delta, \quad (54)$$

where the total comoving density perturbation is given by

$$\rho \Delta = \sum_I \rho_I [\delta_I - 3H(1+w_I)\theta_I], \quad (55)$$

including the vacuum perturbation. The traceless, space-space component of the Einstein field equations, (18), gives the relation between the two scalar potentials in the Newtonian gauge [40]:

$$\psi^N - \phi^N = 8\pi G\Pi, \quad (56)$$

where Π is related to total the anisotropic stresses.

Now the ISW temperature anisotropy is given by the following source:

$$\begin{aligned} S_{ISW} &= \dot{\psi}^N + \dot{\phi}^N \\ &= -8\pi G \frac{d}{dt} \left(\frac{a^2}{k^2} \rho \Delta + \Pi \right). \end{aligned} \quad (57)$$

At late times, the relativistic particles (photons and neutrinos) can be neglected and there is no anisotropic stress. Therefore, it is the comoving density perturbation that drives the late-time ISW effect. Fig. 6 shows how the parameter α affects the time evolution of the gravitational potential in the two models. We see that for the same value of α we find a much larger variation in the Newtonian potential at late times in the barotropic model due to the non-zero sound speed, as shown in Fig. 2. This will be reflected in much tighter bounds on the value of α in the barotropic model coming from the overall CMB anisotropies, and these constraints become even tighter when the galaxy clustering data is also used to identify the late-time ISW effect.

Note that the overall CMB anisotropies, including the ISW effect, is the same in the barotropic model and the original unified Chaplygin gas model since the evolution of the total matter+vacuum density perturbations is the same as the density perturbations in the unified GCG model.

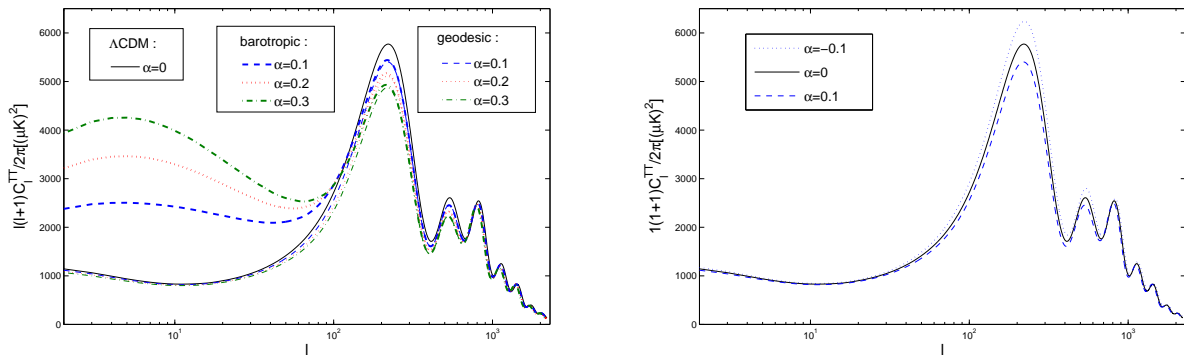


FIG. 5: CMB temperature power spectra vs multipole moment l . The black solid line is for the Λ CDM model. Left panel: Other solid lines and dashed lines for the same values of parameter α correspond to the barotropic model and geodesic model, respectively. Right panel: The dashed line and dotted line correspond to $\alpha = 0.1$ and $\alpha = -0.1$ in the geodesic model, respectively.

In Fig. 7, we present the dark matter power spectrum, the baryonic power spectrum, and the total matter power spectrum (baryon and dark matter) for the barotropic model. The figure shows that, as expected, the dark matter has an oscillating power spectrum in the small-scale limit for non-zero α . The larger the parameter α , the larger the scale where the oscillations of dark matter power spectra begin. By comparison, the baryonic power spectra behave much more smoothly as they are only gravitationally coupled to the oscillating dark matter density [22]. The total matter power spectra combining both dark matter and baryon densities therefore shows intermediate behaviour, but cannot avoid the rapid decay of power spectrum on the small scales for non-zero α .

Fig. 8 shows the total matter power spectra for the geodesic model. The problematic oscillations of the dark matter power spectra do not occur in this case since the sound speed is zero. The only oscillations seen are the baryon acoustic oscillations, also seen in Λ CDM. The matter power spectrum is enhanced on small scales for $\alpha > 0$ due to the earlier matter-radiation equality which moves the turnover in the matter power spectrum to smaller scales.

B. Constraint method and data

Next, we will use a variety of cosmological data to constrain these two models for the matter+vacuum interaction, according to the Markov Chain Monte Carlo (MCMC) method, using the publicly available CosmoMC package [50, 51]. The cosmological parameter set is $P \equiv \{\Omega_b h^2, \Omega_{dm} h^2, \Theta_S, \tau, \alpha, n_s, \log[10^{10} A_s]\}$, where $\Omega_b h^2$ and $\Omega_{dm} h^2$ are the physical baryon and dark matter densities, Θ_S is the ratio (multiplied by 100) of the sound horizon and angular diameter distance, τ is the optical depth, α is the dimensionless generalised Chaplygin

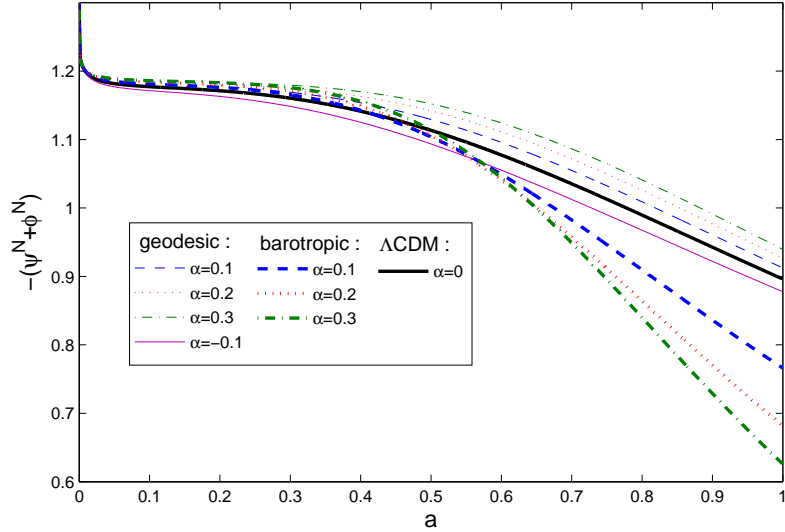


FIG. 6: The evolution of the gravitational potential as a function of scale factor on the large scale $k = 0.001[\text{h Mpc}^{-1}]$. The black solid line is for the ΛCDM model. Other solid lines are for the barotropic model, where the blue line, red line and green line correspond to $\alpha = 0.1, 0.2, 0.3$, respectively. The dashed lines are for the geodesic model, where the blue line, red line and green line correspond to $\alpha = 0.1, 0.2, 0.3$, respectively. The dotted line is the evolution of the gravitational potential for $\alpha = -0.1$ in the geodesic model.

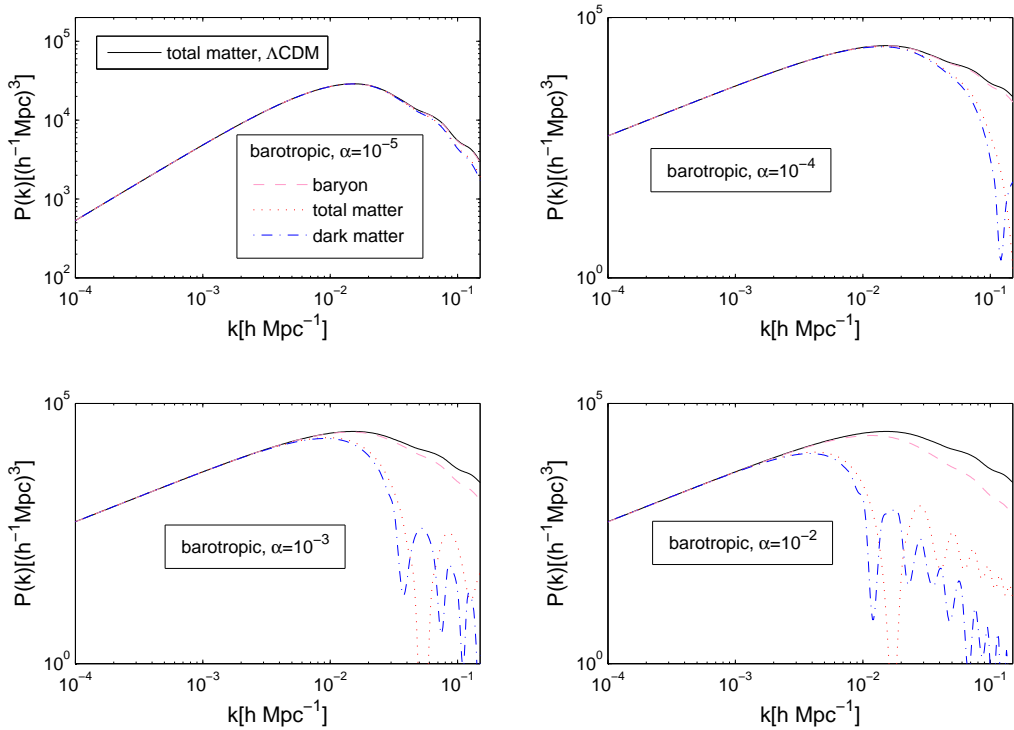


FIG. 7: The LSS power spectra as a function of wavenumber for the barotropic model. On each panel, the black line is the total matter power spectrum for the ΛCDM model. The pink line, red line and blue line are the baryonic power spectrum, the total matter power spectrum and the dark matter power spectrum, respectively. The separate panels (left to right and top to bottom) correspond to $\alpha = 10^{-5}, 10^{-4}, 10^{-3}, 10^{-2}$, respectively.

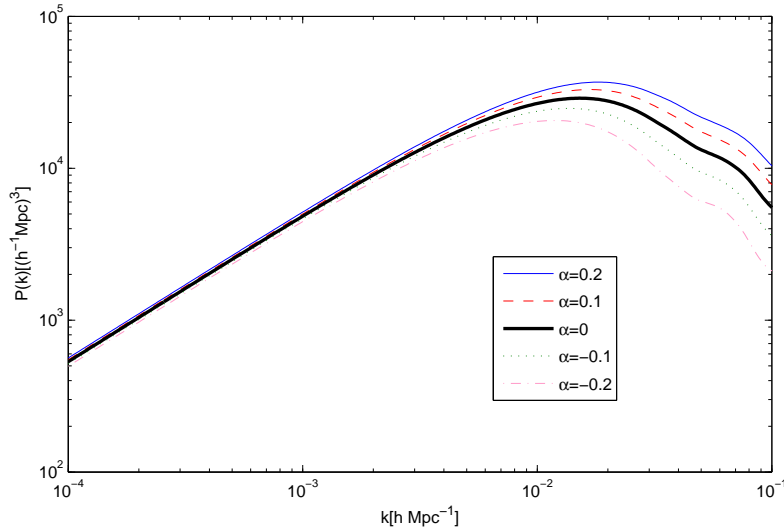


FIG. 8: The total matter power spectra as a function of wavenumber for the geodesic model. The blue line, red line, black line, green line and pink line correspond to $\alpha = 0.2, 0.1, 0$ (Λ CDM model), -0.1, -0.2, respectively.

gas model parameter, n_s is the scalar spectral index, and A_s is defined as the amplitude of the initial power spectrum. Note that the dimensional parameter A in the original definition of the Chaplygin gas (1) is given in terms of Ω_{dm} and Ω_V using Eq. (9) as

$$A = \Omega_V (\Omega_{dm} + \Omega_V)^\alpha \left(\frac{3H_0^2}{8\pi G} \right)^{1+\alpha}, \quad (58)$$

and $\Omega_V = 1 - \Omega_b - \Omega_r - \Omega_{dm}$, by the requirement of spatial flatness.

We will use different combinations of data (CMB+SNIa+BAO, CMB+SNIa+LSS, and CMB+SNIa+gISW). For the LSS power spectra we will only use the linear matter power spectrum up to $k \sim 0.1 [h \text{ Mpc}^{-1}]$. In addition, we use a top-hat prior for the cosmic age, i.e., $10\text{Gyr} < t_0 < 20\text{Gyr}$, impose a weak Gaussian prior on the physical baryon density $\Omega_b h^2 = 0.022 \pm 0.002$ from big bang nucleosynthesis [52], and use the value of the Hubble constant $H_0 = 73.8 \pm 2.4 \text{km s}^{-1} \text{Mpc}^{-1}$ [53] taking a Gaussian likelihood function.

The theoretical galaxy-ISW (gISW) cross-correlated power spectrum, $P_{\delta, \dot{\Phi}}$, where $\dot{\Phi} \equiv \dot{\psi}^N + \dot{\phi}^N$, can be calculated by a modified CAMB code. We modify the code by referring to ISiTGR [54], so that a power spectrum can be directly calculated from the individual transfer function. In the absence of magnification bias, the gISW cross-correlation is written as

$$C_l^{g_x T} = \frac{T_{CMB}}{(l + 1/2)^2} \int dz b_x(z) \Pi_x(z) P_{\delta, \dot{\Phi}} \left(\frac{l + 1/2}{\chi(z)}, z \right), \quad (59)$$

where the galaxy samples in [37] are collected from the Two Micron All Sky Survey (2MASS) Extended Source Catalog (XSC), which is divided into 4 bins: 2MASS0-3, the luminous red galaxies (LRGs) from SDSS split into 2 sample bins: LRG0-1, the photometric quasars from SDSS with 2 redshift bins: QSO0-1, and NRAO VLA Sky Survey (NVSS): NVSS. Namely, there are nine galaxy sample bins x . The scale-independent bias factor $b_x(z)$ is assumed to relate the observed projected galaxy overdensity to the matter density. $\Pi_x(z)$ is the redshift distribution. $\chi(z)$ is the comoving radial distance. In ISWWLL code, the function $f_x(z) \equiv b_x(z) \Pi_x(z)$ is determined by fitting auto power spectra and cross power spectra between the samples:

$$C_l^{g_x g_y} = \int dz f_x(z) f_y(z) D^2(z) P_{\delta, \delta} \left(\frac{l + 1/2}{\chi(z)}, 0 \right), \quad (60)$$

even if the methods differ for the various samples.

For the 2MASS galaxies, the redshifts are identified by matching 2MASS galaxies with SDSS main galaxies. The nonlinear \mathbf{Q} model [55] (denoted by the bold text to be distinguished from the background interaction Q) of the galaxy power spectrum is used to get the bias $b(z)$ and parameter \mathbf{Q} by fitting the auto power spectra of the galaxies to the measured values. For the SDSS LRGs, the redshift distribution is determined by the method in [56], and the bias is also obtained by adopting the same \mathbf{Q} model fitting to the measurements as done for the 2MASS samples. For the SDSS quasars, the preliminary redshift distribution is constructed and is used to predict the shape of the function $f_{QSO0-1}(z)$ in the presence of magnification bias. For NVSS, the analytic Γ distribution for $f_{NVSS}(z)$ is constrained by NVSS auto power spectrum and cross power spectra with other samples.

Parameters	CMB+SNIa+BAO	CMB+SNIa+LSS(m)	CMB+SNIa+gISW	CMB+SNIa+LSS(b)
$\Omega_b h^2$	$0.0225^{+0.0005}_{-0.0005}$	$0.0224^{+0.0005}_{-0.0005}$	$0.0224^{+0.0005}_{-0.0005}$	$0.0224^{+0.0005}_{-0.0005}$
$\Omega_{dm} h^2$	$0.1115^{+0.0033}_{-0.0032}$	$0.1123^{+0.0040}_{-0.0041}$	$0.1102^{+0.0038}_{-0.0038}$	$0.1128^{+0.0034}_{-0.0035}$
Θ_S	$1.0396^{+0.0025}_{-0.0025}$	$1.0394^{+0.0025}_{-0.0025}$	$1.0395^{+0.0025}_{-0.0025}$	$1.0394^{+0.0025}_{-0.0025}$
τ	$0.0872^{+0.0060}_{-0.0067}$	$0.0879^{+0.0061}_{-0.0065}$	$0.0880^{+0.0064}_{-0.0070}$	$0.0865^{+0.0062}_{-0.0069}$
α	$< 2.68 \times 10^{-3}$	$< 1.44 \times 10^{-5}$	$< 3.97 \times 10^{-5}$	$< 3.93 \times 10^{-4}$
n_s	$0.9697^{+0.0127}_{-0.0123}$	$0.9656^{+0.0121}_{-0.0120}$	$0.9667^{+0.0117}_{-0.0118}$	$0.9652^{+0.0122}_{-0.0122}$
$\log[10^{10} A_s]$	$3.0806^{+0.0330}_{-0.0332}$	$3.0835^{+0.0326}_{-0.0333}$	$3.0753^{+0.0343}_{-0.0341}$	$3.0824^{+0.0325}_{-0.0325}$
Ω_V	$0.7321^{+0.0141}_{-0.0139}$	$0.7269^{+0.0200}_{-0.0187}$	$0.7380^{+0.0173}_{-0.0176}$	$0.7244^{+0.0169}_{-0.0169}$
H_0	$70.7674^{+1.2608}_{-1.2489}$	$70.3500^{+1.6739}_{-1.6361}$	$71.2221^{+1.5490}_{-1.5667}$	$70.1242^{+1.4929}_{-1.4919}$

TABLE I: The mean values with 1σ errors and marginalized 95% C. L. of parameter α for the barotropic model using different combinations of data sets.

For each sample, the individual $f_x(z)$ need to be recomputed when the cosmological parameters are changed. We have modified the code [37] to give the correct background evolution for our case, following Eq. (13), and the second-order differential equation for the total matter density perturbation is also modified due to the interaction of the dark matter density perturbation with the vacuum, as given in Eqs. (48) or (53) for our two interaction models. The total matter density contrast is given by

$$\delta_m(z) = \frac{\rho_{dm}\delta_{dm} + \rho_b\delta_b}{\rho_{dm} + \rho_b}. \quad (61)$$

We have checked that compared with the density perturbation, the dark matter velocity term, θ_{dm} , on the right-hand-side of Eq. (48) is small enough to be ignored when we solve the second-order differential equation (48) for the barotropic case.

C. Barotropic model constraints

We present the constraints for the barotropic model from the combined data sets of CMB+SNIa+BAO, CMB+SNIa+LSS(m), CMB+SNIa+gISW, and CMB+SNIa+LSS(b) in Table I. Here LSS(b) denotes the constraints obtained by fitting the LSS power spectra to the baryonic matter power spectra, while LSS(m) means that the theoretical predictions for the total matter (baryon+dark matter) power spectra are used. The corresponding 1D marginal distribution of the parameter α and the 2D contour plots of the parameters α and Ω_V are shown in Fig. 9.

From the Table I and Fig. 9, we can see that the joint data from CMB+SNIa+BAO can constrain α to be less than or of order 10^{-3} . Tighter bounds on the parameter α can be obtained by using the LSS power spectra data. When the total matter power spectra are used to fit the SDSS DR7 power spectra data combined with data from CMB+SNIa, the tightest bounds on the parameter α are obtained, to less than or of order 10^{-5} . By comparison when the baryonic power spectra are fitted to the SDSS DR7 power spectra data, larger values of α are allowed and the upper limit at 95% confidence level (C. L.) is 3.93×10^{-4} . This is because the dark matter power spectra are damped on small scales more quickly than the baryonic power spectra as shown in Fig. 7. From the solid lines on the left panel of Fig. 5, it is seen that the low-multipole CMB power spectrum for the barotropic model is obviously enhanced with the increasing α through the ISW effect. By using the data of CMB+SNIa+gISW, we obtain $\alpha < 3.97 \times 10^{-5}$ at the 95% C. L..

D. Geodesic model constraints

For the geodesic model, the constraints from the combination of various data are listed in Table II. The marginal 1D distributions and 2D contour plots from CMB+SNIa+BAO, CMB+SNIa+LSS(m), and CMB+SNIa+gISW are shown in Fig. 10.

CMB+SNIa+LSS(m) constraints allow negative mean value for α . Compared with results from CMB+SNIa+BAO and CMB+SNIa+LSS(m) constraints, CMB+SNIa+gISW gives a relatively narrow allowed range for α . The allowed range of the parameter α at the 95% C. L. in this case are $-0.1606 < \alpha < 0.3042$ from CMB+SNIa+BAO, $-0.2111 < \alpha < 0.2069$ from CMB+SNIa+LSS(m) and $-0.1522 < \alpha < 0.2557$ from CMB+SNIa+gISW, respectively. By comparison with the results for the barotropic model on the basis of the same data sets, the allowed region of parameter α for the geodesic model is obviously enlarged.

Finally, in Fig. 11 we show gISW cross-correlation power spectra predicted by using the mean values of CMB+SNIa+gISW for the two models.

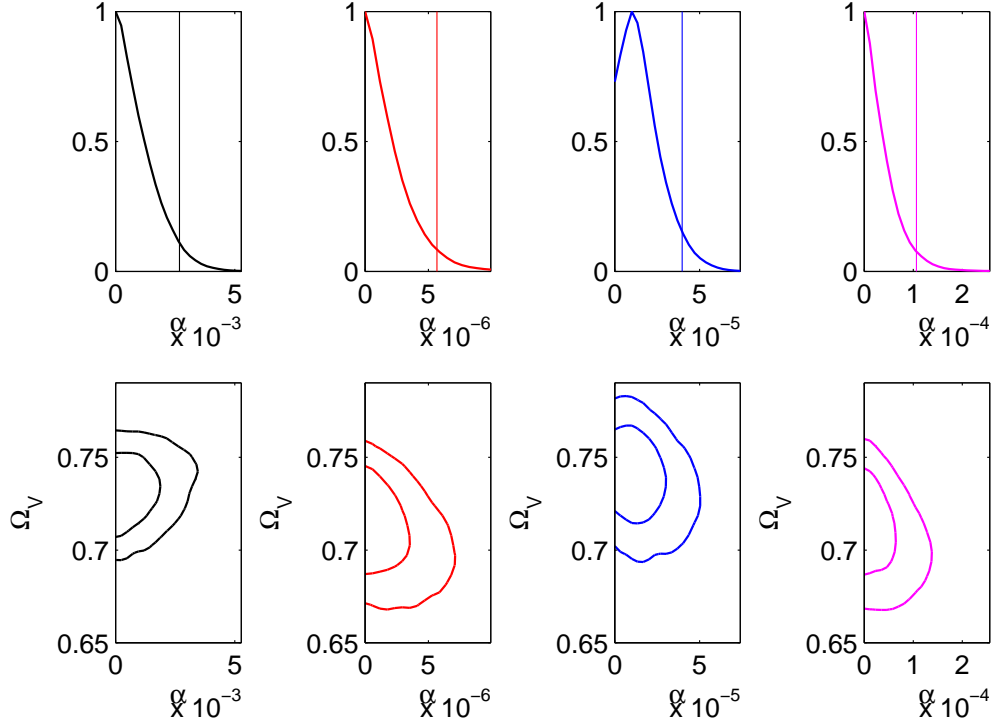


FIG. 9: The 1D marginalized distributions for the parameter α and 2D contours with 68% C. L. and 95% C. L. for the barotropic model using the combinations of CMB+BAO+SNIa (black line), CMB+SNIa+LSS(m) (red line), CMB+SNIa+gISW (blue line) and CMB+SNIa+LSS(b) (magenta line), respectively. The vertical lines on the top panels are the 95% confident levels.

Parameters	CMB+SNIa+BAO	CMB+SNIa+LSS(m)	CMB+SNIa+gISW
$\Omega_b h^2$	$0.0224^{+0.0005}_{-0.0005}$	$0.0224^{+0.0005}_{-0.0005}$	$0.0225^{+0.0005}_{-0.0005}$
$\Omega_{dm} h^2$	$0.1077^{+0.0144}_{-0.0146}$	$0.1167^{+0.0148}_{-0.0147}$	$0.1062^{+0.0135}_{-0.0135}$
Θ_S	$1.0395^{+0.0026}_{-0.0026}$	$1.0393^{+0.0026}_{-0.0026}$	$1.0397^{+0.0025}_{-0.0025}$
τ	$0.0864^{+0.0063}_{-0.0072}$	$0.0875^{+0.0066}_{-0.0073}$	$0.0895^{+0.0065}_{-0.0076}$
α	$0.0388^{+0.1138}_{-0.1134}$	$-0.0227^{+0.1029}_{-0.1036}$	$0.0272^{+0.1017}_{-0.1013}$
n_s	$0.9636^{+0.0126}_{-0.0128}$	$0.9656^{+0.0129}_{-0.0128}$	$0.9665^{+0.0127}_{-0.0125}$
$\log[10^{10} A_s]$	$3.0812^{+0.0334}_{-0.0331}$	$3.0825^{+0.0335}_{-0.0335}$	$3.0762^{+0.0342}_{-0.0344}$
Ω_V	$0.7381^{+0.0379}_{-0.0375}$	$0.7116^{+0.0436}_{-0.0436}$	$0.7494^{+0.0346}_{-0.0347}$
H_0	$70.6346^{+1.4753}_{-1.4671}$	$69.6824^{+1.9423}_{-1.9394}$	$71.8121^{+1.7092}_{-1.7111}$

TABLE II: The mean values with 1σ errors for the geodesic model using different combinations of data sets.

V. CONCLUSIONS

Any unified dark matter model can be decomposed into dark matter interacting with vacuum energy [30–32]. In such a decomposed model, the vacuum energy is coupled to dark matter and the energy-momentum transfer between the vacuum energy and the dark matter is given by the gradient of vacuum energy. Different covariant forms for the energy-momentum transfer four-vector have different effects on the CMB angular power spectrum and LSS power spectrum through the different evolution of inhomogeneous perturbation evolutions, even if the background cosmology is the same. Observational constraints on these decomposed models correspond to constraints on the interaction between dark matter and the vacuum energy, where we recover Λ CDM in the limit of zero interaction.

In this paper, we studied the evolution of perturbations in a decomposed Chaplygin gas model and compared this with the evolution in a unified Chaplygin gas model with adiabatic perturbations. We considered two different models for the energy-momentum transfer in the decomposed case. In one model the energy-momentum transfer is along the gradient of the local dark matter density, in which case we recover the evolution equations for perturbations of a single barotropic fluid with the same equation of state as the generalised Chaplygin gas.

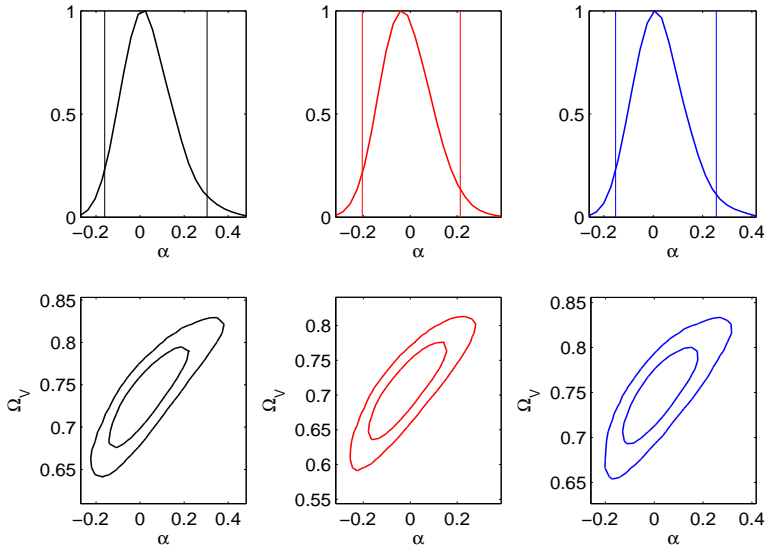


FIG. 10: The 1D marginalized distributions for the parameter α and 2D contours with 68% C. L. and 95% C. L. for the geodesic model using the combinations of CMB+SNIa+BAO (black line), CMB+SNIa+LSS(m) (red line), and CMB+SNIa+gISW (blue line), respectively. The vertical lines on the top panels are the 95% confident levels.

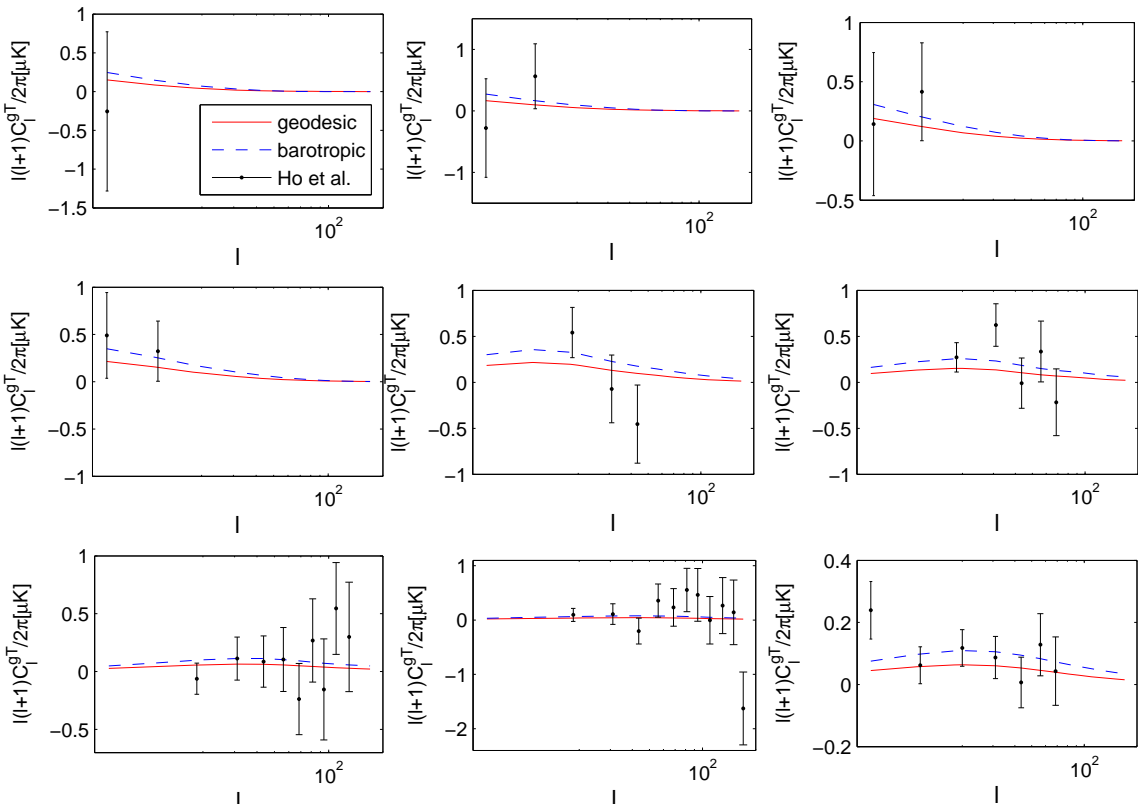


FIG. 11: The gISW cross-correlation power spectra with different galaxy samples for the barotropic model (blue line) with mean values taken from CMB+SNIa+gISW constraints in the Table I and the geodesic model (red line) with mean values taken from CMB+SNIa+gISW constraints in the Table II, respectively. The black dots with error bars denote the gISW data from Ho et al. [37].

The pressure perturbations are adiabatic and the rest-frame sound speed equals the adiabatic sound speed. This non-zero sound speed has an effect on both the CMB power spectrum and the LSS power spectrum. Increasing α enhances the CMB power spectra at the low multipoles. In addition, the effect on the total matter (baryon+dark matter) power spectrum caused by the sound speed is that there are decaying oscillations in the matter power spectrum for positive α , as for the generalised Chaplygin gas [20].

A different possibility which we considered is that the energy-momentum transfer is along the dark matter four-velocity, which leads to the dark matter following geodesics. Compared with the barotropic model, the geodesic model has a relative entropy perturbation between dark matter and vacuum energy. Thus the sound speed of the interacting dark matter+vacuum energy in the dark matter rest frame is zero. There are no oscillations or instabilities in the total matter power spectrum for positive or negative α .

In the decomposed Chaplygin gas, different interaction models can lead to very different evolution of perturbations due to the different sound speeds. We test whether these two kinds of decomposed models can be supported or distinguished by current observations. We have constrained the barotropic model and geodesic model by using various combinations of data sets, including CMB constraints, type Ia supernovae, BAO distance measurements, large-scale structure and the integrated Sachs-Wolfe effect..

For the barotropic model the most stringent constraint on the α parameter is of the order of 10^{-5} from the combinations of CMB+SNIa+LSS(m), where the theoretical total matter (baryon+dark matter) power spectrum is fitted to the LSS power spectrum data. We conclude that a barotropic model must be extremely close to the Λ CDM model. In contrast the allowed region for the α parameter in the geodesic model is much and larger α , and negative α , can also be compatible with the observations. The geodesic model thus allows significant deviations from the Λ CDM model.

In the case of a unified dark matter model it is not clear whether the galaxy power spectrum on large scales should follow the total matter power spectrum, which gives rise to the gravitaitonal potential, or the baryonic matter power spectrum, since only baryons follow geodesics. This choice leads to different predictions for the LSS power spectrum [22]. The same ambiguity applies in our barotropic model of interacting vacuum+dark matter, since the dark matter does not follow geodesics in this case, so we present constraints using LSS fitted to both the total matter power spectrum and the baryonic matter power spectrum. In the geodesic model, however, we only use the total matter power spectrum to fit the LSS power spectrum since both the dark matter and the baryons follow geodesics in this case and we expect the total matter overdensity to be responsible for the formation of collapsed halos. Nonetheless it would be interesting to study further the process of non-linear collapse in this model and we hope to return to this question in future work.

Acknowledgments

YW would like to thank Timothy Clemson, Lucas Lombriser, Gong-Bo Zhao for help with the CosmoMC and ISWWLL code. DW is supported by STFC grant ST/H002774/1. Xu is supported by NSF (11275035). JD-S is supported by CONACYT grant 210405. AH is supported by World Class University grant R32-2009-000-10130-0 through the National Research Foundation, Ministry of Education, Science and Technology of Korea. All the numerical computations were done on the Sciamia High Performance Compute cluster, supported by the ICG SEPNet and University of Portsmouth. YW and JD-S thank the ICG, University of Portsmouth for their hospitality.

- [1] M. Makler, S. Q. de Oliveira and I. Waga, Phys. Lett. B **555**, 1 (2003) [astro-ph/0209486].
- [2] M. C. Bento, O. Bertolami and A. A. Sen, Phys. Rev. D **66**, 043507 (2002) [gr-qc/0202064].
- [3] A. Y. Kamenshchik, U. Moschella and V. Pasquier, Phys. Lett. B **511**, 265 (2001) [gr-qc/0103004]; N. Bilic, G. B. Tupper and R. D. Viollier, Phys. Lett. B **535**, 17 (2002) [astro-ph/0111325].
- [4] M. Biesiada, W. Godlowski and M. Szydłowski, Astrophys. J. **622**, 28 (2005) [astro-ph/0403305].
- [5] R. Colistete and J. C. Fabris, Class. Quant. Grav. **22**, 2813 (2005) [astro-ph/0501519].
- [6] M. C. Bento, O. Bertolami, M. J. Reboucas and P. T. Silva, Phys. Rev. D **73**, 043504 (2006) [gr-qc/0512158].
- [7] M. C. Bento, O. Bertolami and A. A. Sen, Phys. Rev. D **67**, 063003 (2003) [astro-ph/0210468].
- [8] M. C. Bento, O. Bertolami and A. A. Sen, Phys. Lett. B **575**, 172 (2003) [astro-ph/0303538].
- [9] M. C. Bento, O. Bertolami and A. A. Sen, Gen. Rel. Grav. **35**, 2063 (2003) [gr-qc/0305086].
- [10] Z. H. Zhu, Astron. Astrophys. **423**, 421 (2004) [astro-ph/0411039].
- [11] P. Wu and H. Yu, Phys. Lett. B **644**, 16 (2007) [gr-qc/0612055].
- [12] J. C. Fabris, P. L. C. de Oliveira and H. E. S. Velten, arXiv:1106.0645 [astro-ph.CO].
- [13] Z. Li, P. Wu and H. Yu, JCAP **09**, 017 (2009) [arXiv:0908.3415[astro-ph.CO]].
- [14] O. Bertolami and P. T. Silva, astro-ph/0601507.
- [15] J. V. Cunha, J. S. Alcaniz and J. A. S. Lima, Phys. Rev. D **69**, 083501 (2004) [astro-ph/0306319]; J. S. Alcaniz and J. A. S. Lima, Astrophys. J. **618** 16 (2005), Astrophys. J. **618**, 16 (2004) [astro-ph/0308465].
Y. Gong, JCAP **0503**, 007 (2005) [astro-ph/0411253].
- P. Wu and H. Yu, JCAP **0703**, 015 (2007) [astro-ph/0701446].

J. Lu, Y. Gui and L. Xu, Eur. Phys. J. C **63**, 349 (2009) [arXiv:1004.3365[astro-ph.CO]].
 L. Xu and J. Lu, JCAP **1003** 025 (2010) [arXiv:1004.3344[astro-ph.CO]].
 N. Liang, L. Xu and Z. H. Zhu Astronomy & Astrophysics, **527**, A11 (2011) [arXiv:1009.6059[astro-ph.CO]].

[16] R. K. Sachs and A. M. Wolfe, Astrophys. J. **147**, 73 (1967).
 [17] D. Carturan and F. Finelli, Phys. Rev. D **68**, 103501 (2003) [astro-ph/0211626].
 [18] L. Amendola, F. Finelli, C. Burigana and D. Carturan, JCAP **0307**, 005 (2003) [astro-ph/0304325].
 [19] L. Xu, J. Lu and Y. Wang, Eur. Phys. J. C **72**, 1883 (2012) [arXiv:1204.4798].
 [20] H. Sandvik, M. Tegmark, M. Zaldarriaga and I. Waga, Phys. Rev. D **69**, 123524 (2004) [astro-ph/0212114].
 [21] M. Colless *et al.*, Mon. Not. Roy. Astron. Soc. **328**, 1039 (2001) [astro-ph/0106498v3];
 M. Tegmark, A. J. S. Hamilton and Y. Xu, Mon. Not. Roy. Astron. Soc. **335**, 887 (2002) [astro-ph/0111575].
 [22] C. -G. Park, J. -c. Hwang, J. Park and H. Noh, Phys. Rev. D **81**, 063532 (2010) [arXiv:0910.4202 [astro-ph.CO]].
 [23] O. F. Piattella, D. Bertacca, M. Bruni and D. Pietrobon, JCAP **1001**, 014 (2010) [arXiv:0911.2664 [astro-ph.CO]].
 [24] D. Bertacca, M. Bruni, O. F. Piattella and D. Pietrobon, JCAP **1102**, 018 (2011) [arXiv:1011.6669 [astro-ph.CO]].
 [25] R. R. R. Reis, I. Waga, M. O. Calvao and S. E. Joras Phys. Rev. D **68**, 061302 (2003) [astro-ph/0306004].
 [26] L. Amendola, I. Waga and F. Finelli, JCAP **0511**, 009 (2005) [astro-ph/0509099].
 [27] E. Gaztañaga, M. Manera and T. Multamaki, Mon. Not. Roy. Astron. Soc. **365**, 171 (2006) [astro-ph/0407022].
 [28] T. Giannantonio and A. Melchiorri, Class. Quant. Grav. **23**, 4125 (2006) [gr-qc/0606030].
 [29] W. Zimdahl and J. C. Fabris Class. Quant. Grav. **22**, 4311 (2005) [gr-qc/0504088].
 [30] M. C. Bento, O. Bertolami and A. A. Sen, Phys. Rev. D **70**, 083519 (2004) [astro-ph/0407239].
 [31] D. Wands, J. De-Santiago and Y. Wang, Class. Quant. Grav. **29**, 145017 (2012) [arXiv:1203.6776 [astro-ph.CO]].
 [32] J. De-Santiago, D. Wands and Y. Wang, arXiv:1209.0563 [astro-ph.CO].
 [33] E. Komatsu *et al.*, Astrophys. J. Suppl. **192**, 18 (2011) [arXiv:1001.4538[astro-ph.CO]];
 <http://lambda.gsfc.nasa.gov/product/map/current/>.
 [34] N. Suzuki *et al.*, ApJ, **746**, 85 (2012) [arXiv:1105.3470[astro-ph.CO]].
 [35] W. J. Percival *et al.*, Mon. Not. Roy. Astron. Soc. **401**, 2148 (2010) [arXiv:0907.1660[astro-ph.CO]].
 [36] B. A. Reid *et al.*, Mon. Not. Roy. Astron. Soc. **404**, 60 (2010) [arXiv:0907.1659[astro-ph.CO]].
 [37] S. Ho, C. Hirata, N. Padmanabhan, U. Seljak and N. Bahcall, Phys. Rev. D **78**, 043519 (2008) [arXiv:0801.0642].
 [38] V. F. Mukhanov, H. A. Feldman and R. H. Brandenberger, Phys. Rept. **215** (1992) 203-333.
 [39] K. A. Malik, astro-ph/0101563.
 [40] K. A. Malik and D. Wands, Phys. Rept. **475**, 1 (2009) [arXiv:0809.4944[astro-ph.CO]].
 [41] K. A. Malik and D. Wands, JCAP **0502**, 007 (2005) [astro-ph/0411703].
 [42] H. Kodama and M. Sasaki, Prog. Theor. Phys. Suppl. **78**, 1 (1984).
 [43] K. A. Malik, D. Wands and C. Ungarelli, Phys. Rev. D **67**, 063516 (2003) [astro-ph/0211602].
 [44] <http://camb.info/>.
 [45] C. P. Ma and E. Bertschinger, Astrophys. J. **455**, 7 (1995) [astro-ph/9506072].
 [46] R. Bean and O. Doré, Phys. Rev. D **68**, 023515 (2003) [astro-ph/0301308].
 [47] R. Bean, E. E. Flanagan, I. Laszlo and M. Trodden, Phys. Rev. D **78**, 123514 (2008) [arXiv:0808.1105[astro-ph.CO]].
 J. Q. Xia, Phys. Rev. D **80**, 103514 (2009) [arXiv:0911.4820[astro-ph.CO]].
 [48] J. Valiviita, E. Majerotto and R. Maartens, JCAP **0807**, 020 (2008) [arXiv:0804.0232[astro-ph.CO]].
 [49] K. Koyama, R. Maartens and Y. S. Song, JCAP **0910**, 017 (2009) [arXiv:0907.2126[astro-ph.CO]].
 [50] A. Lewis and S. Bridle, Phys. Rev. D **66**, 103511 (2002) [astro-ph/0205436].
 [51] <http://cosmologist.info/cosmomc/>.
 [52] S. Burles, K. M. Nollett and M. S. Turner, Astrophys. J. **552**, L1 (2001).
 [53] A. G. Riess *et al.*, ApJ, **730**, 119 (2011) [arXiv:1103.2976[astro-ph.CO]].
 [54] J. Dossett, M. Ishak and J. Moldenhauer, Phys. Rev. D **84**, 123001 (2011) [arXiv:1109.4583[astro-ph.CO]];
 J. Dossett and M. Ishak, Phys. Rev. D **86**, 103008 (2012) [arXiv:1205.2422[astro-ph.CO]].
 [55] S. Cole *et al.*, Mon. Not. Roy. Astron. Soc. **362**, 505 (2005) [astro-ph/0501174].
 [56] N. Padmanabhan *et al.*, Mon. Not. Roy. Astron. Soc. **359**, 237 (2005) [astro-ph/0407594].

Cosmological constraints on a decomposed Chaplygin gas

Yuting Wang^{1,2}, David Wands², Lixin Xu¹, Josue De-Santiago^{3,2} and Alireza Hojjati⁴

¹*School of Physics and Optoelectronic Technology, Dalian University of Technology,
Dalian, Liaoning 116024, People's Republic of China*

²*Institute of Cosmology and Gravitation, University of Portsmouth, Portsmouth, PO1 3FX, United Kingdom*

³*Universidad Nacional Autónoma de México, 04510, Distrito Federal, México*

⁴*Institute for the Early Universe, Ewha Womans University, Seoul, 120-750, South Korea*

(Dated: April 5, 2013)

Any unified dark matter cosmology can be decomposed into dark matter interacting with vacuum energy, without introducing any additional degrees of freedom. We present observational constraints on an interacting vacuum plus dark energy corresponding to a generalised Chaplygin gas cosmology. We consider two distinct models for the interaction leading to either a barotropic equation of state or dark matter that follows geodesics, corresponding to a rest-frame sound speed equal to the adiabatic sound speed or zero sound speed, respectively. For the barotropic model, the most stringent constraint on α comes from the combination of CMB+SNIa+LSS(m) gives $\alpha < 5.66 \times 10^{-6}$ at the 95% confidence level, which indicates that the barotropic model must be extremely close to the Λ CDM cosmology. For the case where the dark matter follows geodesics, perturbations have zero sound speed, and CMB+SNIa+gISW then gives the much weaker constraint $-0.15 < \alpha < 0.26$ at the 95% confidence level.

I. INTRODUCTION

The dominance of dark energy and dark matter in the present cosmological energy density has led many authors to seek a unified description in terms of a single dark component, referred to as unified dark matter or quartessence [1], which should explain both the current accelerated expansion of the Universe and the role of nonbaryonic dark matter in structure formation. One candidate from this kind of model, which has attracted a lot of attention, is the generalized Chaplygin gas (GCG) model [2, 3]. It is a fluid, defined by an exotic equation of state,

$$P_{gCg} = -\frac{A}{\rho_{gCg}^\alpha}, \quad (1)$$

with model parameters α and A . The GCG model with $\alpha = 1$ reduces to the original Chaplygin gas model [2, 4]. Predictions of the GCG cosmology has been tested against the different observational data, including type Ia supernovae (SNIa) [5–7], the positions of cosmic microwave background (CMB) radiation peaks [8–10], the X-ray gas mass fraction of clusters [11], Hubble parameter-redshift data [12, 13], the lookback time-redshift data [14], gamma-ray bursts [15], and as well as various combinations of the updated data [16].

Going beyond constraints provided by the homogeneous background cosmology, the inclusion of inhomogeneous linear perturbations in the GCG has an effect on both the cosmic microwave background anisotropies and structure formation. In particular, the imprint of a large integrated Sachs-Wolfe (ISW) signal [17], which arises from a time-dependent gravitational potential when dark energy dominates at late times in the Universe, could be observed on the CMB anisotropies [18, 19]. Recently, in Ref. [20] two of us revisited constraints on the GCG model from the combination of CMB, baryon acoustic oscillations (BAO), and SNIa, including the full CMB temperature and polarization power spectra data. A tight bound for the parameter α was obtained up to the order of 10^{-3} .

The effect of the GCG on structure formation also contains important information. In Ref. [21], it was argued that in order to predict large-scale structure (LSS) consistent with the data from the 2dF survey [22], the GCG model has to be indistinguishable from Λ CDM, with $\alpha < \mathcal{O}(10^{-5})$. The slightly looser constraint, $\alpha < \mathcal{O}(10^{-4})$ was obtained in Ref. [23] by fitting the predicted baryon matter power spectrum, rather than the total matter power spectrum, to the Sloan Digital Sky Survey (SDSS) DR7 power spectrum data¹. In either case a stringent limit is placed on the α parameter because there are either instabilities or oscillations in the GCG power spectra due to the adiabatic pressure perturbation produced for nonzero α . This problem can be avoided in some unified dark matter models by requiring a fast transition between a CDM-like era and a Λ CDM-like phase [25–27].

In order to save the GCG model some type of intrinsic entropy perturbation must be introduced in the GCG fluid to counteract the effect caused by the adiabatic GCG pressure perturbation, as in the so-called silent GCG model [28]. The combined constraints from data on both the silent GCG and standard GCG model are presented in Ref. [29]. It is shown that with a vanishing GCG pressure perturbation there is a much wider allowed parameter range, $-0.3 < \alpha < 0.7$ [29]. Subsequently, the ISW data [30] was used to constrain the silent

¹ The theoretical baryon power spectrum may also be compatible with SDSS observations for large $\alpha > 1$, corresponding to a superluminal sound speed [24], however the CMB power spectrum does not favour this regime [23].

GCG model [31]. The required entropy perturbation can be introduced by decomposing the GCG fluid into two components of dark matter and dark energy [32], but the possible ways of decomposition are not unique [33]. In Ref. [34] the GCG model was split into dark matter and vacuum energy, considering a homogeneous vacuum when studying density perturbations in the Newtonian limit.

Recently it has been shown that any unified dark matter model can be decomposed into dark matter interacting with a vacuum energy (with equation of state $P = -\rho$) without introducing any additional degrees of freedom [35]. In general an interacting vacuum energy is inhomogenous, and a description of the dynamics of inhomogeneous vacuum energy was presented in Refs. [35, 36].

In this paper we will study in detail the constraints on a decomposed GCG model described by dark matter interacting with inhomogeneous vacuum energy. A closed set of perturbation equations are obtained once a covariant form is specified for the interaction. Firstly, we consider a model in which the vacuum energy is a function of the local matter density. We show this leads to a barotropic equation of state for the dark matter+vacuum, and hence reproduces previous results for a unified GCG. Secondly we consider an energy-momentum transfer parallel to the matter four-velocity, leading to a geodesic flow for the matter. In both cases we consider background cosmologies that mimic the GCG cosmologies, but the evolution of linear perturbations differs due to the presence of non-adiabatic pressure perturbations. We pay particular attention to their imprints on the CMB and LSS power spectra. To constrain the barotropic and geodesic model parameters we will use different combinations of current cosmological data including the CMB temperature and polarization power spectra [37], SNIa from the Union2.1 compilation of the Supernova Cosmology Project Collaboration [38], the BAO distance measurements [39], the LSS power spectrum from SDSS DR7 [40], and the galaxy-ISW (gISW) cross-correlation power spectra from Ref. [41].

This paper is organized as follows. In the next section, we review the background equations for the GCG model. In Sec. III, the linear perturbation equations for both the unified GCG model and the two decomposed models are presented. In Sec. IV, we show the effects on CMB and LSS power spectra in the two decomposed models, then perform a global fitting to observational data by using the Markov Chain Monte Carlo (MCMC) method and discuss the resulting constraints on the interaction. In the final section we present our conclusions. In what follows (unless otherwise specified) the illustrative plots are shown using the joint mean values for cosmological parameters from WMAP7 data [37]: $\Omega_b h^2 = 0.02255$, $\Omega_{dm} h^2 = 0.1126$, $h = 0.702$, $\tau = 0.088$, $n_s = 0.968$, and $A_s = 2.43 \times 10^{-9}$ at $k_{s0} = 0.002 \text{ Mpc}^{-1}$.

II. CHAPLYGIN GAS COSMOLOGY

We will consider a spatially flat, homogeneous and isotropic Friedmann-Robertson-Walker universe with metric

$$ds^2 = -dt^2 + a^2(t)\delta_{ij}dx^i dx^j, \quad (2)$$

where the Friedmann equation is given by

$$H^2 \equiv \left(\frac{\dot{a}}{a}\right)^2 = \frac{8\pi G}{3}(\rho_b + \rho_r + \rho_{gCg}), \quad (3)$$

where ρ_b , ρ_r and ρ_{gCg} are the energy densities of baryons, radiation and a generalised Chaplygin gas which can act as both a dark energy component, accelerating the Universe at late times, and dark matter. The energy conservation equations for the various components read

$$\dot{\rho}_b + 3H\rho_b = 0, \quad (4)$$

$$\dot{\rho}_r + 4H\rho_r = 0, \quad (5)$$

$$\dot{\rho}_{gCg} + 3H(\rho_{gCg} + P_{gCg}) = 0. \quad (6)$$

The equation of state for GCG (1) then allows us to integrate Eq. (6) to obtain

$$\rho_{gCg} = \rho_{gCg0} \left[B_s + (1 - B_s)a^{-3(1+\alpha)} \right]^{1/(1+\alpha)}, \quad (7)$$

where ρ_{gCg0} is the present value of energy density of GCG (when $a = a_0 = 1$) and we have replaced A in Eq. (1) with the dimensionless model parameter, $B_s = A/\rho_{gCg0}^{1+\alpha}$.

In a previous work we have shown that a unified dark matter fluid with an arbitrary equation of state can be decomposed into pressureless dark matter interacting with a vacuum energy, V , with an appropriate energy transfer [35] (see also Ref. [33]). For the GCG solution (7), we can write

$$\rho_{gCg} = \rho_{dm} + V, \quad (8)$$

such that, from Eq. (1)

$$A = V(\rho_{dm} + V)^\alpha. \quad (9)$$

The conservation equations of dark matter and vacuum energy are

$$\dot{\rho}_{dm} + 3H\rho_{dm} = -Q, \quad (10)$$

$$\dot{V} = Q. \quad (11)$$

Thus from Eqs. (9)-(11), we obtain

$$Q = 3\alpha H \frac{\rho_{dm} V}{\rho_{dm} + V}. \quad (12)$$

In the decomposed model (8), the parameter, B_s in Eq. (7), can be written in terms of the present values of the energy densities, $B_s = [V/(\rho_{dm} + V)]_0$. The decomposed model is characterised by a single dimensionless parameter α [35], but an FRW solution is specified by two boundary conditions (such as the present density of matter and vacuum) whereas the original GCG model is specified by two model parameters, α and A (or B_s) and one boundary condition. This already suggests that the decomposed model may naturally accommodate nonadiabatic density perturbations, in addition to the adiabatic perturbations of the original GCG. As we shall see, this can have important consequences for the evolution of perturbations in a decomposed model.

Note that the Friedmann equation (3) can be written as

$$H^2 = H_0^2 \left\{ \Omega_b a^{-3} + \Omega_r a^{-4} + (\Omega_V + \Omega_{dm}) \left[\frac{\Omega_V}{\Omega_V + \Omega_{dm}} + \frac{\Omega_{dm}}{\Omega_V + \Omega_{dm}} a^{-3(1+\alpha)} \right]^{\frac{1}{1+\alpha}} \right\}, \quad (13)$$

where the dimensionless fractional energy density of individual components is defined as

$$\Omega_I = \left(\frac{8\pi G \rho_I}{3H^2} \right)_0, \quad (14)$$

which satisfies $\Omega_b + \Omega_r + \Omega_V + \Omega_{dm} = 1$.

We illustrate the background evolution as a function of redshift for different values of the parameter α in Fig. 1. In the particular case when $\alpha = 0$, the background evolution is identical to that for the Λ CDM model.

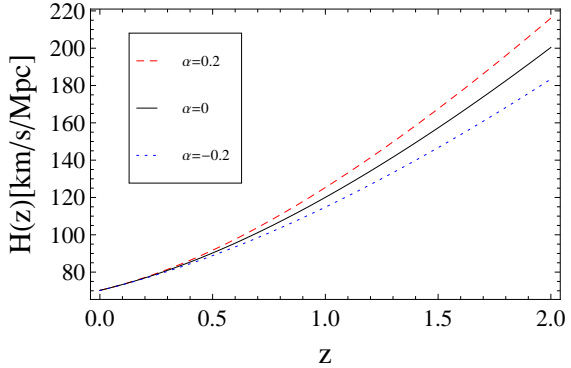


FIG. 1: The Hubble parameter as a function of redshift z for different values of parameter α , where the solid line with $\alpha = 0$ corresponds to Λ CDM model.

The FRW background solution, Eq. (13), shows a degeneracy between the decomposed vacuum+dark matter with the interaction (12) and the unified GCG with equation of state (1), where $\Omega_{gCg} = \Omega_V + \Omega_{dm}$ and $B_s = \Omega_V/(\Omega_V + \Omega_{dm})$. As discussed in Ref. [33], this is an example of a more general degeneracy between interacting and unified models. One can either specify an exotic equation of state for a unified dark matter model, or one can obtain many equivalent decomposed models containing interacting fluids with a specified energy transfer. Although equivalent to a unified model at the background level, we expect different physical models for the interaction to be distinguished by the evolution of inhomogeneous perturbations.

III. THE LINEAR PERTURBATION EQUATIONS

We begin with a general scalar mode of the metric perturbation in an arbitrary gauge with the perturbed line of element [42–45]

$$ds^2 = -(1 + 2\phi)dt^2 + 2a\partial_i B dt dx^i + a^2 [(1 - 2\psi)\delta_{ij} + 2\partial_i \partial_j E] dx^i dx^j. \quad (15)$$

The Einstein equations are [42–45]

$$3H(\dot{\psi} + H\phi) - \frac{\nabla^2}{a^2}(\psi + H\sigma) = -4\pi G\delta\rho, \quad (16)$$

$$\dot{\psi} + H\phi = -4\pi G(\rho + P)\theta, \quad (17)$$

$$\dot{\sigma} + H\sigma - \phi + \psi = 8\pi G\Pi, \quad (18)$$

$$\ddot{\psi} + 3H\dot{\psi} + H\dot{\phi} + (3H^2 + 2\dot{H})\phi = 4\pi G\left(\delta P + \frac{2}{3}\frac{\nabla^2}{a^2}\Pi\right), \quad (19)$$

where $\sigma \equiv a^2\dot{E} - aB$ is the shear, $\delta\rho$ is the total density perturbation, δP is the total pressure perturbation, Π is the total anisotropic stress, and θ is the total covariant velocity perturbation².

For each individual component, the covariant conservation equation allowing for energy-momentum transfer gives

$$\nabla_\mu T_{(I)}^{\mu\nu} = Q_{(I)}^\nu. \quad (20)$$

General relativity requires conservation of the total energy-momentum, $\nabla_\mu T^{\mu\nu} = 0$, so we have $\sum_I Q_{(I)}^\nu = 0$. The perturbed energy-momentum transfer four-vector is conventionally split into the energy transfer, $Q_I + \delta Q_I$, and momentum transfer, f_I , relative to the total four-velocity [44–47]

$$Q_\mu^{(I)} = [-Q_I(1 + \phi) - \delta Q_I, \partial_i(f_I + Q_I\theta)]. \quad (21)$$

The energy and momentum conservation equations for each fluid component are then [43–45, 47]:

$$\dot{\delta\rho}_I + 3H(\delta\rho_I + \delta P_I) - 3(\rho_I + P_I)\dot{\psi} + (\rho_I + P_I)\frac{\nabla^2}{a^2}(\theta_I + \sigma) = \delta Q_I + Q_I\phi, \quad (22)$$

$$(\rho_I + P_I)\dot{\theta}_I - 3c_{sI}^2 H(\rho_I + P_I)\theta_I + (\rho_I + P_I)\phi + \delta P_I + \frac{2}{3}\frac{\nabla^2}{a^2}\Pi_I = f_I + Q_I\theta - (1 + c_{sI}^2)Q_I\theta_I, \quad (23)$$

where $c_{sI}^2 = \dot{P}_I/\dot{\rho}_I$ is the adiabatic sound speed.

The numerical code CAMB [48] is written in the synchronous gauge, so in order to place quantitative constraints on the model parameters we will solve the equations in a synchronous gauge [49] where

$$\phi = B = 0, \quad \psi = \eta, \quad \text{and} \quad k^2 E = -\frac{h}{2} - 3\eta. \quad (24)$$

There is a residual spatial gauge freedom in the synchronous gauge which allows one to set the initial velocity of any component to zero. We see from Eq. (23) that it is possible to work in a gauge in which $\theta_I = 0$ at all times for non-interacting, pressureless matter. A comoving synchronous gauge is commonly used, in which the dark matter velocity is zero, $\theta_{dm} = 0$. This is no longer possible in models where the dark matter experiences a momentum transfer, $f_{dm} + Q_{dm}(\theta - \theta_{dm}) \neq 0$. We can still work in a synchronous gauge, but note that the dark matter velocity is not necessarily zero.

The time-time and time-space components of the perturbed Einstein field equations, (16) and (17), in the synchronous gauge are

$$\frac{\dot{h}}{2} = \frac{1}{H}\left(\frac{k^2}{a^2}\eta + 4\pi G\delta\rho\right), \quad (25)$$

$$\dot{\eta} = -4\pi G(\rho + P)\theta. \quad (26)$$

Together with the energy and momentum conservation equations for each component, these form a closed set of equations.

After decoupling, the baryon component is conserved independently and the perturbation equations for the baryon density contrast and velocity are given by

$$\dot{\delta}_b - \frac{k^2}{a^2}\theta_b = -\frac{\dot{h}}{2}, \quad (27)$$

$$\dot{\theta}_b = 0. \quad (28)$$

Combining Eqs. (18), (19) in the synchronous gauge and Eq. (25), we have

$$\ddot{h} + 2H\dot{h} = -8\pi G(\delta\rho + 3\delta P). \quad (29)$$

By differentiating Eq. (27) with respect to time and combining Eq. (28) and the above equation, we find a second-order differential equation for the baryonic density contrast,

$$\ddot{\delta}_b + 2H\dot{\delta}_b = 4\pi G(\delta\rho + 3\delta P). \quad (30)$$

² Note that $\theta \equiv a(v + B)$ in terms of the total velocity potential v defined in, e.g., Ref. [45].

A. Unified GCG model

First let us consider perturbations in the unified GCG model, where the energy-momentum tensor of the GCG is conserved and hence Eqs. (22) and (23) give the perturbed energy and momentum conservation equations

$$\dot{\delta}_{gCg} + 3H(c_{s,gCg}^2 - w_{gCg})\delta_{gCg} + (1 + w_{gCg})\left(-\frac{k^2}{a^2}\theta_{gCg} + \frac{\dot{h}}{2}\right) = 0, \quad (31)$$

$$\dot{\theta}_{gCg} - 3c_{s,gCg}^2 H\theta_{gCg} + \frac{c_{s,gCg}^2}{1 + w_{gCg}}\delta_{gCg} = 0, \quad (32)$$

where the adiabatic sound speed for the GCG is fixed by the equation of state of the GCG

$$c_{s,gCg}^2 = -\alpha w_{gCg}, \quad (33)$$

$$w_{gCg} = -\frac{B_s}{B_s + (1 - B_s)a^{-3(1+\alpha)}}. \quad (34)$$

We can derive a second-order differential equation for GCG overdensity by differentiating Eq. (31) with respect to time and combining Eqs. (29) and (32),

$$\begin{aligned} \ddot{\delta}_{gCg} &+ 2H[1 + 3(c_{s,gCg}^2 - w_{gCg})]\dot{\delta}_{gCg} \\ &+ [3\dot{H}(c_{s,gCg}^2 - w_{gCg}) + 3H(c_{s,gCg}^2 - w_{gCg}) + 9H^2(c_{s,gCg}^2 - w_{gCg})^2 + 6H^2(c_{s,gCg}^2 - w_{gCg})]\delta_{gCg} \\ &= -c_{s,gCg}^2 \frac{k^2}{a^2} \delta_{gCg} + (1 + w_{gCg})3c_{s,gCg}^2 H \frac{k^2}{a^2} \theta_{gCg} + (1 + w_{gCg})4\pi G(\delta\rho + 3\delta P). \end{aligned} \quad (35)$$

The first term on the right-hand-side of the above equation dominates in the small-scale limit and the adiabatic pressure perturbation causes the instabilities (or oscillations) of density perturbations for negative (or positive) α [50].

B. Interacting vacuum energy + dark matter models

Let us now consider a general interacting vacuum energy + dark matter model, where the energy continuity equations (22) for the dark matter and vacuum energy in the synchronous gauge become

$$\dot{\delta\rho}_{dm} + 3H\delta\rho_{dm} + \rho_{dm}\left(-\frac{k^2}{a^2}\theta_{dm} + \frac{\dot{h}}{2}\right) = \delta Q_{dm}, \quad (36)$$

$$\dot{\delta V} = \delta Q_V, \quad (37)$$

while the momentum conservation equations (23) are given by

$$\rho_{dm}\dot{\theta}_{dm} = f_{dm} + Q_{dm}(\theta - \theta_{dm}), \quad (38)$$

$$-\delta V = f_V + Q_V\theta. \quad (39)$$

Note that the vacuum energy has vanishing momentum and therefore the force exerted on the vacuum, $\partial_i(f_V + Q_V\theta)$, is exactly canceled by the gradient of the vacuum pressure, $\partial_i(-\delta V)$.

The conservation of total energy-momentum for the interacting dark matter and vacuum energy implies that

$$Q_V = -Q_{dm} = Q, \quad \delta Q_V = -\delta Q_{dm}, \quad f_V = -f_{dm}. \quad (40)$$

We can then eliminate δQ_{dm} and f_{dm} using the energy and momentum conservation equations for the vacuum (37) and (39) to leave the energy-momentum conservation equations for the dark matter

$$\dot{\delta}_{dm} - \frac{Q}{\rho_{dm}}\delta_{dm} - \frac{k^2}{a^2}\theta_{dm} + \frac{\dot{h}}{2} = -\frac{\dot{\delta V}}{\rho_{dm}} \quad (41)$$

$$\rho_{dm}\dot{\theta}_{dm} = \delta V + Q\theta_{dm}, \quad (42)$$

where the background energy transfer Q is given by Eq. (12).

Note that the interacting vacuum+dark matter introduces no additional degrees of freedom with respect to the original GCG. We have two coupled first-order equations (41) and (42) for the dark matter density and velocity, instead of the two coupled first-order equations (31) and (32) for the GCG density and velocity. The background solution determines the adiabatic sound speed and equation of state for the GCG, whereas a

physical model for the interaction is required to determine the vacuum perturbation, δV , and can affect the sound speed for the interacting vacuum+dark matter.

Generally we can identify two classes of interacting models which could be used to specify the energy-momentum transfer in the decomposed model. Either one can specify the vacuum energy as a function, $V(X)$, of some scalar quantity X , and hence $\delta V = V'(X)\delta X$. Or else one can identify a four-vector, U^μ , which the energy-transfer (20) is parallel to: $Q_V^\mu \propto U^\mu$. In the following we will consider one example of each class of interacting model, but we note that these are not unique and it may be interesting to consider other possibilities with different observational signatures.

1. Barotropic model

Firstly, we consider a model in which the vacuum energy density is a function of local dark matter density

$$V = V(\rho_{dm}) . \quad (43)$$

This implies that the energy transfer between the vacuum and the dark matter is along the gradient of the local dark matter density: $Q_V^\mu \propto \nabla^\mu \rho_{dm}$.

At linear order, we have

$$\delta V = \frac{\dot{V}}{\dot{\rho}_{dm}} \delta \rho_{dm} , \quad (44)$$

which shows that in this case the relative perturbations between the vacuum and the dark matter are adiabatic. The total pressure perturbation for the interacting dark matter+vacuum energy is

$$\begin{aligned} -\delta V &= \frac{\alpha V}{\rho_{dm} + V} (\delta \rho_{dm} + \delta V) \\ &= c_{s,gCg}^2 (\delta \rho_{dm} + \delta V) . \end{aligned} \quad (45)$$

Therefore, the sound speed for the interacting dark matter+vacuum energy is exactly the same as the adiabatic sound speed for the original generalised Chaplygin gas, $c_{s,gCg}^2$ given by Eq. (33) [35, 36]. We show the effect on the sound speed caused by the parameter α in Fig. 2.

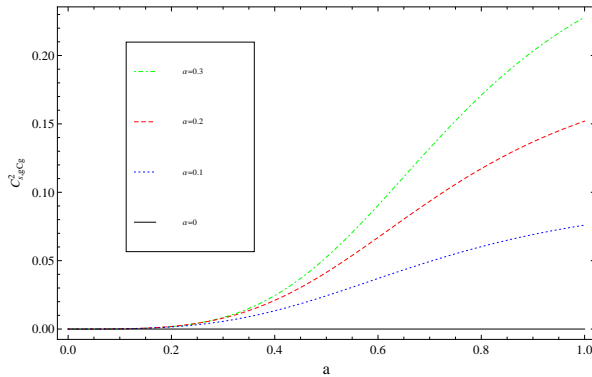


FIG. 2: The sound speed as a function of scale factor a for the barotropic model.

In the synchronous gauge, we have from Eqs. (41), (42) and (44)

$$\dot{\delta}_{dm} = \frac{(1+\alpha)Q}{\rho_{dm} + (1+\alpha)V} \delta_{dm} + \frac{\rho_{dm} + (1+\alpha)V}{\rho_{dm} + V} \frac{k^2}{a^2} \theta_{dm} - \frac{\rho_{dm} + (1+\alpha)V}{\rho_{dm} + V} \frac{\dot{h}}{2} , \quad (46)$$

$$\dot{\theta}_{dm} = \frac{Q}{\rho_{dm}} \theta_{dm} - \frac{\alpha V}{\rho_{dm} + (1+\alpha)V} \delta_{dm} , \quad (47)$$

It is clear that the barotropic model with $\alpha = 0$ reduces to the Λ CDM model at the linear order. Comparing with dark matter perturbations in the standard Λ CDM model, we can see that density contrasts and velocities of the interacting dark matter evolve very differently. In this case, due to the presence of momentum transfer, θ_{dm} will evolve to be nonzero, even if its initial value is set to zero. Therefore, the synchronous gauge is not comoving with the interacting dark matter and we calculate the perturbed equations in an arbitrary synchronous gauge [51].

Combining Eqs. (46) and (47) with Eq. (29), we obtain a second-order differential equation for the dark matter overdensity

$$\begin{aligned} \ddot{\delta}_{dm} &= \left[\frac{2(1+\alpha)Q}{\rho_{dm} + (1+\alpha)V} - 2H \right] \dot{\delta}_{dm} \\ &- \left\{ \left[\frac{(1+\alpha)Q}{\rho_{dm} + (1+\alpha)V} \right] \dot{\delta}_{dm} - \left[\frac{(1+\alpha)Q}{\rho_{dm} + (1+\alpha)V} \right]^2 + 2H \left[\frac{(1+\alpha)Q}{\rho_{dm} + (1+\alpha)V} \right] \right\} \delta_{dm} \\ &= -c_{s,gCg}^2 \frac{k^2}{a^2} \delta_{dm} + \left(1 + \frac{\alpha V}{\rho_{dm} + V} \right) \frac{Q}{\rho_{dm}} \frac{k^2}{a^2} \theta_{dm} + \left(1 + \frac{\alpha V}{\rho_{dm} + V} \right) 4\pi G(\delta\rho + 3\delta P). \end{aligned} \quad (48)$$

The first term on the right-hand-side of Eq. (48) dominates in the small-scale limit. Negative α causes instabilities of density perturbations. Conversely, there are oscillations of perturbations for positive α . In order to avoid the presence of negative sound speed, we will require $\alpha \geq 0$ in this case.

We find that the perturbations for the barotropic model, Eqs. (46)-(48), obey the same dynamical evolutions as those for the unified GCG model, Eqs. (31), (32) and (35), where we identify

$$\delta_{gCg} = \frac{\rho_{dm}}{\rho_{dm} + (1+\alpha)V} \delta_{dm}, \quad \theta_{gCg} = \theta_{dm}. \quad (49)$$

We should not be surprised that this interacting model reproduces the same behaviour as the GCG since by requiring $V = V(\rho_{dm})$ we have set the pressure of the interacting matter+vacuum $P_{dm+V} = -V$ to be an implicit function of $\rho_{dm} + V$, i.e., we have a barotropic fluid.

The evolution of the dark matter density perturbations for the barotropic model on a fixed scale is shown in Fig. 3. In the left panel, it is shown that increasing α causes the suppression of the growth of density fluctuations on the scale, $k = 0.001 [\text{h Mpc}^{-1}]$. For the smaller scale, $k = 0.01 [\text{h Mpc}^{-1}]$, in the right panel, we can see that density fluctuations rapidly decay and oscillate with increasing α .

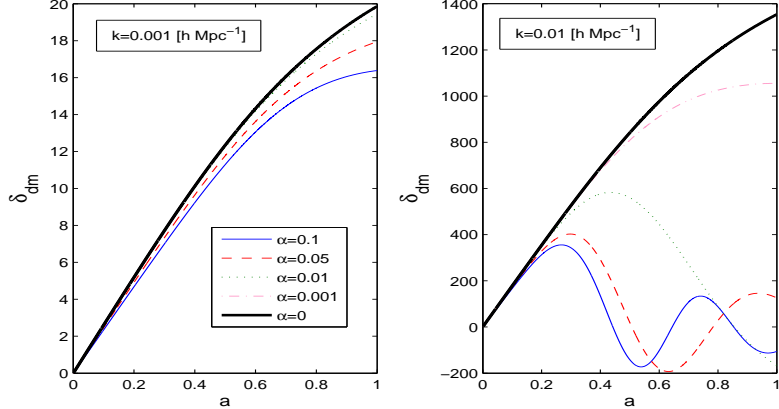


FIG. 3: The dark matter density perturbations on fixed scales: $k = 0.001 [\text{h Mpc}^{-1}]$ (left panel) and $k = 0.01 [\text{h Mpc}^{-1}]$ (right panel) as a function of scale factor for the barotropic model. The thin solid line, dashed line, dotted line, dot-dashed line and thick solid line correspond to $\alpha = 0.1, 0.05, 0.01, 0.001, 0$ (Λ CDM model), respectively.

2. Geodesic model

An alternative model for the energy transfer is to consider an energy flow that is parallel to the four-velocity of the dark matter:

$$Q_{(dm)}^\mu = -Qu_{(dm)}^\mu. \quad (50)$$

For this form of the covariant interaction there is no momentum transfer in the rest frame of dark matter [52, 53], $f_{dm} - Q(\theta - \theta_{dm}) = 0$ in Eq. (21). The velocity perturbation for dark matter is not affected by the interaction and obeys the standard equation, $\dot{\theta}_{dm} = 0$ from Eq. (38). This allows us to work in a synchronous gauge that is comoving with the dark matter ($\theta_{dm} = 0$). The dark matter four-velocity, u^μ is thus a geodesic flow: $u_{(dm)}^\mu \nabla_\mu u_{(dm)}^\nu = 0$. Hence we will refer to this form of energy-transfer as a geodesic model.

The vacuum perturbation in the dark matter-comoving frame is identically zero, from Eq. (42),

$$\delta V_{com} = \delta V + \dot{V}\theta_{dm} = 0. \quad (51)$$

The pressure perturbation for the interacting vacuum+dark matter is therefore zero in the dark matter rest frame and thus the speed of sound for the interacting vacuum+dark matter is zero³ [35, 36]. Note that this implies that in this case there is a non-adiabatic pressure perturbation, due to the relative entropy perturbation between the dark matter and the vacuum energy [35, 36], in contrast to the barotropic model.

From Eq. (41), the perturbation equation for the dark matter density contrast in the rest frame of dark matter obeys

$$\dot{\delta}_{dm} = -\frac{\dot{h}}{2} + \frac{Q}{\rho_{dm}} \delta_{dm}. \quad (52)$$

We see that, again, the case with $\alpha = 0$ is completely equivalent to Λ CDM at linear order.

A second-order differential equation for the dark matter overdensity can be derived from the above equation and Eq. (29), which gives

$$\ddot{\delta}_{dm} + \left(-\frac{Q}{\rho_{dm}} + 2H \right) \dot{\delta}_{dm} - \left[2H \frac{Q}{\rho_{dm}} + \left(\frac{\dot{Q}}{\rho_{dm}} \right) \right] \delta_{dm} = 4\pi G(\delta\rho + 3\delta P). \quad (53)$$

We plot the evolution of the dark matter density perturbations on different scales in Fig. 4. Compared with the growth in the Λ CDM model, positive α indicates that there is an energy transfer from dark matter to vacuum energy, so the growth of density perturbations with positive α is suppressed at early times during matter-domination. At late times, vacuum energy dominates in the Universe, and the vacuum interaction drives the growth of dark matter density perturbations. Conversely, for the negative α the growth of density perturbations is enhanced at early times and is gradually suppressed at late times. Note that there is no instability associated with imaginary speed of sound for $\alpha < 0$ in the geodesic model.

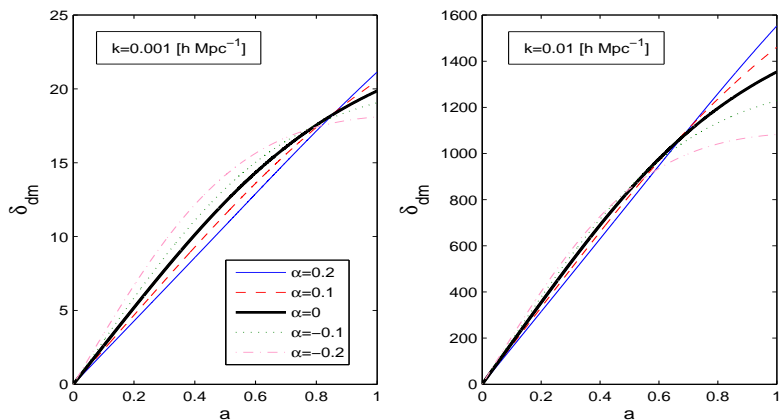


FIG. 4: The dark matter density perturbations on fixed scales: $k = 0.001$ [$h \text{ Mpc}^{-1}$] (left panel) and $k = 0.01$ [$h \text{ Mpc}^{-1}$] (right panel) as a function of scale factor for the geodesic model. The thin solid line, dashed line, thick solid line, dotted line and dot-dashed line correspond to $\alpha = 0.2, 0.1, 0$ (Λ CDM model), $-0.1, -0.2$, respectively.

IV. COSMOLOGICAL CONSTRAINTS

A. Theoretical predictions of CMB and LSS power spectra

First, we illustrate the imprint on the CMB and LSS power spectra for different values of the parameter α for both the barotropic model and geodesic model. For the barotropic model we will restrict the value of α to be greater than or equal to zero in order to avoid instabilities due to an imaginary sound speed, but we will extend α to negative values for the geodesic model since the sound speed remains real in that case.

The effects on the CMB power spectra are shown in Fig. 5. From the left panel, positive α leads to an energy transfer from dark matter to vacuum energy. Increasing α causes the matter-radiation equality to

³ A vanishing pressure perturbation was also considered in a Cardassian model without any internal fluctuations, which in a special case that $\nu = 1$ reproduces a GCG background [54]. However we will show that in the geodesic model dark matter density perturbations are affected by the background interaction and obey a modified perturbation equation.

happen earlier and hence suppresses the first acoustic peaks. Conversely, negative α delays the epoch of matter-radiation equality, and hence amplifies the acoustic peaks, as shown in the geodesic case in the right panel of Fig. 5.

One source of CMB anisotropies at low multipoles is the ISW effect. The amplitude of the ISW signal on large scales is affected not only by the epoch of dark matter-vacuum energy equality, but is also modified directly by the evolution of the gravitational potential, which differs in the barotropic and geodesic models. These two competing mechanisms give the final ISW signal.

In order to clearly express the ISW effect caused by the time-varying gravitational potential, we calculate the Newtonian potential, ψ^N , corresponding to the metric perturbation, ψ , in the Newtonian or longitudinal gauge ($B = E = 0$) [49].

This is given by the relativistic Poisson equation [44]

$$k^2 \psi^N = -4\pi G a^2 \rho \Delta, \quad (54)$$

where the total comoving density perturbation is given by

$$\rho \Delta = \sum_I \rho_I [\delta_I - 3H(1+w_I)\theta_I], \quad (55)$$

including the vacuum perturbation. The traceless, space-space component of the Einstein field equations, (18), gives the relation between the two scalar potentials in the Newtonian gauge [44]:

$$\psi^N - \phi^N = 8\pi G \Pi, \quad (56)$$

where Π is related to total the anisotropic stresses.

Now the ISW temperature anisotropy is given by the following source:

$$\begin{aligned} S_{ISW} &= \dot{\psi}^N + \dot{\phi}^N \\ &= -8\pi G \frac{d}{dt} \left(\frac{a^2}{k^2} \rho \Delta + \Pi \right). \end{aligned} \quad (57)$$

At late times, the relativistic particles (photons and neutrinos) can be neglected and there is no anisotropic stress. Therefore, it is the comoving density perturbation that drives the late-time ISW effect. Figure 6 shows how the parameter α affects the time evolution of the gravitational potential in the two models. We see that for the same value of α we find a much larger variation in the Newtonian potential at late times in the barotropic model due to the nonzero sound speed, as shown in Fig. 2. This will be reflected in much tighter bounds on the value of α in the barotropic model coming from the overall CMB anisotropies, and these constraints become even tighter when the galaxy clustering data is also used to identify the late-time ISW effect.

Note that the overall CMB anisotropies, including the ISW effect, are the same in the barotropic model and the original unified Chaplygin gas model⁴ since the evolution of the total matter+vacuum density perturbations is the same as the density perturbations in the unified GCG model.

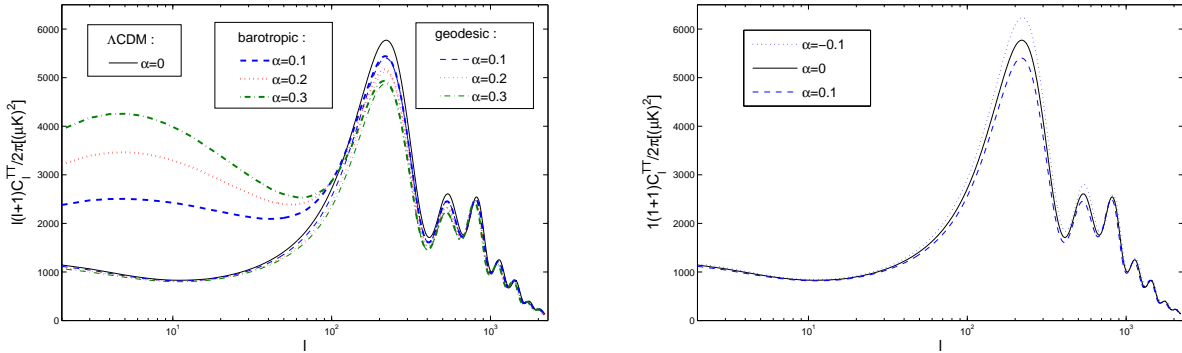


FIG. 5: CMB temperature power spectra vs multipole moment l . The solid line is for the Λ CDM model. Left panel: The thick lines and thin lines for the same values of parameter α correspond to the barotropic model and geodesic model, respectively. Right panel: The dashed line and dotted line correspond to $\alpha = 0.1$ and $\alpha = -0.1$ in the geodesic model, respectively.

⁴ This case can also be obtained from case II of the Cardassian model in Ref. [54] for $\nu = 1$.

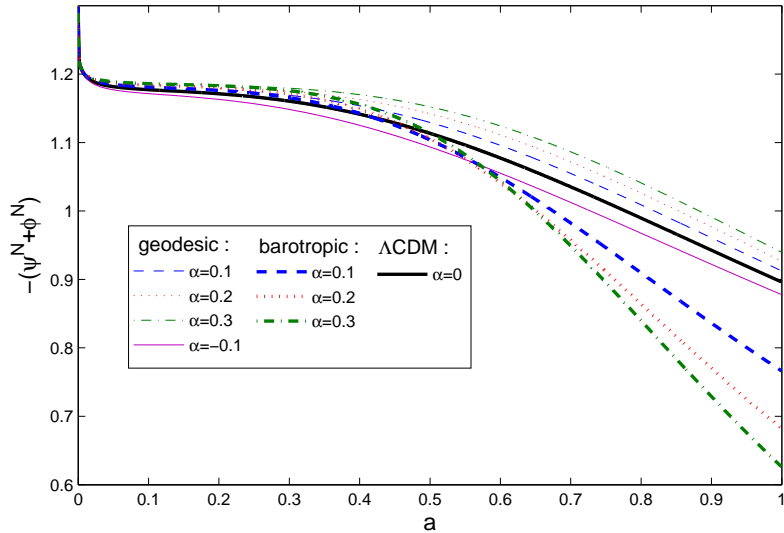


FIG. 6: The evolution of the gravitational potential as a function of scale factor on the large scale $k = 0.001[h \text{ Mpc}^{-1}]$. The thick solid line is for the ΛCDM model. The thick dashed, dotted and dot-dashed lines correspond to $\alpha = 0.1, 0.2, 0.3$ for the barotropic model, respectively. The thin dashed, dotted and dot-dashed lines correspond to $\alpha = 0.1, 0.2, 0.3$ for the geodesic model, respectively. The thin solid line is the evolution of the gravitational potential for $\alpha = -0.1$ in the geodesic model.

In Fig. 7, we present the dark matter power spectrum, the baryonic power spectrum, and the total matter power spectrum (baryon and dark matter) for the barotropic model. The figure shows that, as expected, the dark matter has an oscillating power spectrum in the small-scale limit for nonzero α . The larger the parameter α , the larger the scale where the oscillations of dark matter power spectra begin. By comparison, the baryonic power spectra behave much more smoothly as they are only gravitationally coupled to the oscillating dark matter density [23]. The total matter power spectra combining both dark matter and baryon densities therefore shows intermediate behaviour, but cannot avoid the rapid decay of power spectrum on the small scales for nonzero α .

Figure 8 shows the total matter power spectra for the geodesic model. The problematic oscillations of the dark matter power spectra do not occur in this case since the sound speed is zero. The only oscillations seen are the baryon acoustic oscillations, also seen in ΛCDM . The matter power spectrum is enhanced on small scales for $\alpha > 0$ due to the earlier matter-radiation equality which moves the turnover in the matter power spectrum to smaller scales.

B. Constraint method and data

Next, we will use a variety of cosmological data to constrain these two models for the matter+vacuum interaction, according to the Markov Chain Monte Carlo method, using the publicly available CosmoMC package [55, 56]. The cosmological parameter set is $P \equiv \{\Omega_b h^2, \Omega_{dm} h^2, \Theta_S, \tau, \alpha, n_s, \log[10^{10} A_s]\}$, where $\Omega_b h^2$ and $\Omega_{dm} h^2$ are the physical baryon and dark matter densities, Θ_S is the ratio (multiplied by 100) of the sound horizon and angular diameter distance, τ is the optical depth, α is the dimensionless generalised Chaplygin gas model parameter, n_s is the scalar spectral index, and A_s is defined as the amplitude of the initial power spectrum. Note that the dimensional parameter A in the original definition of the Chaplygin gas (1) is given in terms of Ω_{dm} and Ω_V using Eq. (9) as

$$A = \Omega_V (\Omega_{dm} + \Omega_V)^\alpha \left(\frac{3H_0^2}{8\pi G} \right)^{1+\alpha}, \quad (58)$$

and $\Omega_V = 1 - \Omega_b - \Omega_r - \Omega_{dm}$, by the requirement of spatial flatness.

We will use different combinations of data (CMB+SNIa+BAO, CMB+SNIa+LSS, and CMB+SNIa+gISW). For the LSS power spectra we will only use the linear matter power spectrum up to $k \sim 0.1[h \text{ Mpc}^{-1}]$. In addition, we use a top-hat prior for the cosmic age, i.e., $10\text{Gyr} < t_0 < 20\text{Gyr}$, impose a weak Gaussian prior on the physical baryon density $\Omega_b h^2 = 0.022 \pm 0.002$ from big bang nucleosynthesis [57], and use the value of the Hubble constant $H_0 = 73.8 \pm 2.4 \text{km s}^{-1} \text{Mpc}^{-1}$ [58] taking a Gaussian likelihood function.

The theoretical galaxy-ISW (gISW) cross-correlated power spectrum, $P_{\delta, \dot{\Phi}}$, where $\dot{\Phi} \equiv \dot{\psi}^N + \dot{\phi}^N$, can be calculated by a modified CAMB code. We modify the code by referring to ISiTGR [59], so that a power

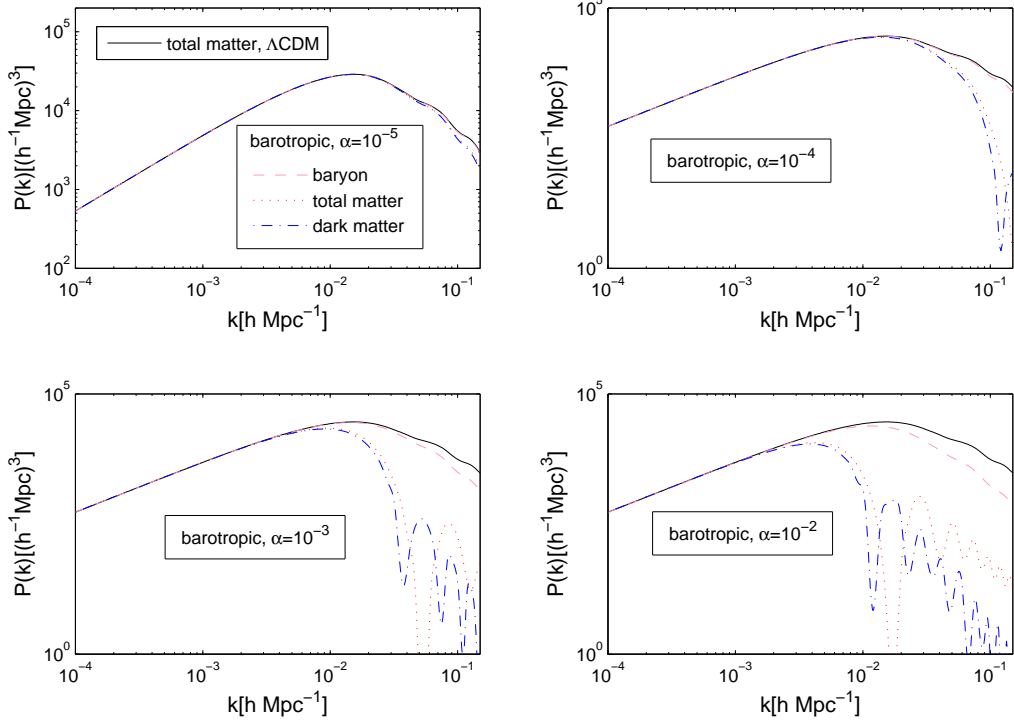


FIG. 7: The LSS power spectra as a function of wavenumber for the barotropic model. In each panel, the solid line is the total matter power spectrum for the Λ CDM model. The dashed line, dotted line and dot-dashed line are the baryonic power spectrum, the total matter power spectrum and the dark matter power spectrum, respectively. The separate panels (left to right and top to bottom) correspond to $\alpha = 10^{-5}, 10^{-4}, 10^{-3}, 10^{-2}$, respectively.

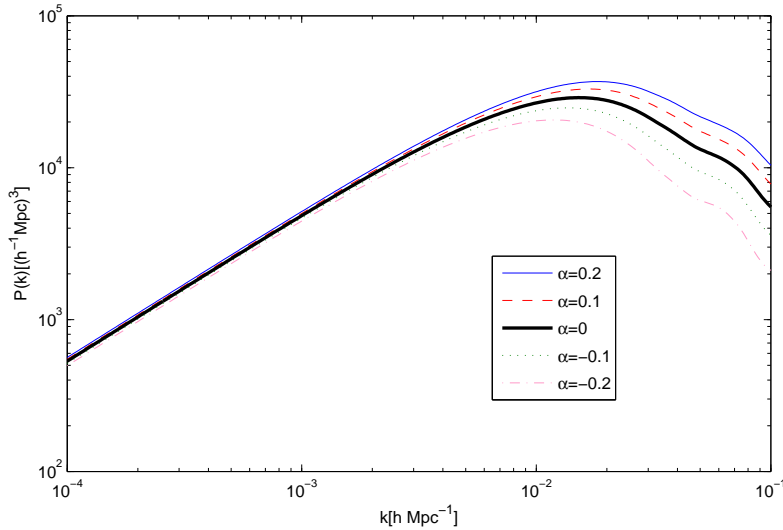


FIG. 8: The total matter power spectra as a function of wavenumber for the geodesic model. The thin solid line, dashed line, thick solid line, dotted line and dot-dashed line correspond to $\alpha = 0.2, 0.1, 0$ (Λ CDM model), -0.1, -0.2, respectively.

spectrum can be directly calculated from the individual transfer function. In the absence of magnification bias, the gISW cross correlation is written as

$$C_l^{g_x T} = \frac{T_{CMB}}{(l+1/2)^2} \int dz b_x(z) \Pi_x(z) P_{\delta, \dot{\Phi}} \left(\frac{l+1/2}{\chi(z)}, z \right), \quad (59)$$

where the galaxy samples in Ref. [41] are collected from the Two Micron All Sky Survey (2MASS) Extended Source Catalog (XSC), which is divided into 4 bins: 2MASS0-3, the luminous red galaxies (LRGs) from SDSS

split into 2 sample bins: LRG0-1, the photometric quasars from SDSS with 2 redshift bins: QSO0-1, and NRAO VLA Sky Survey (NVSS): NVSS. Namely, there are nine galaxy sample bins x . The scale-independent bias factor $b_x(z)$ is assumed to relate the observed projected galaxy overdensity to the matter density. $\Pi_x(z)$ is the redshift distribution. $\chi(z)$ is the comoving radial distance. In ISWWLL code, the function $f_x(z) \equiv b_x(z)\Pi_x(z)$ is determined by fitting auto power spectra and cross power spectra between the samples:

$$C_l^{g_x g_y} = \int dz f_x(z) f_y(z) \frac{H(z)}{\chi^2(z)} D^2(z) P_{\delta, \delta} \left(\frac{l+1/2}{\chi(z)}, 0 \right), \quad (60)$$

even if the methods differ for the various samples.

For the 2MASS galaxies, the redshifts are identified by matching 2MASS galaxies with SDSS main galaxies. The nonlinear \mathbf{Q} model [60] (denoted by the bold text to be distinguished from the background interaction Q) of the galaxy power spectrum is used to get the bias $b(z)$ and parameter \mathbf{Q} by fitting the auto power spectra of the galaxies to the measured values. For the SDSS LRGs, the redshift distribution is determined by the method in Ref. [61], and the bias is also obtained by adopting the same \mathbf{Q} model fitting to the measurements as done for the 2MASS samples. For the SDSS quasars, the preliminary redshift distribution is constructed and is used to predict the shape of the function $f_{QSO0-1}(z)$ in the presence of magnification bias. For NVSS, the analytic Γ distribution for $f_{NVSS}(z)$ is constrained by NVSS auto power spectrum and cross power spectra with other samples.

For each sample, the individual $f_x(z)$ need to be recomputed when the cosmological parameters are changed. We have modified the code [41] to give the correct background evolution for our case, following Eq. (13), and the second-order differential equation for the total matter density perturbation is also modified due to the interaction of the dark matter density perturbation with the vacuum, as given in Eqs. (48) or (53) for our two interaction models. The total matter density contrast is given by

$$\delta_m(z) = \frac{\rho_{dm}\delta_{dm} + \rho_b\delta_b}{\rho_{dm} + \rho_b}. \quad (61)$$

We have checked that compared with the density perturbation, the dark matter velocity term, θ_{dm} , on the right-hand-side of Eq. (48) is small enough to be ignored when we solve the second-order differential equation (48) for the barotropic case.

C. Barotropic model constraints

We present the constraints for the barotropic model from the combined data sets of CMB+SNIa+BAO, CMB+SNIa+LSS(m), CMB+SNIa+gISW, and CMB+SNIa+LSS(b) in Table I. Here LSS(b) denotes the constraints obtained by fitting the LSS power spectra to the baryonic matter power spectra, while LSS(m) means that the theoretical predictions for the total matter (baryon+dark matter) power spectra are used. The corresponding 1D marginal distribution of the parameter α and the 2D contour plots of the parameters α and Ω_V are shown in Fig. 9.

From Table I and Fig. 9, we can see that the joint data from CMB+SNIa+BAO can constrain α to be less than or of order 10^{-3} . Tighter bounds on the parameter α can be obtained by using the LSS power spectra data. When the total matter power spectra are used to fit the SDSS DR7 power spectra data combined with data from CMB+SNIa, the tightest bounds on the parameter α are obtained, to less than or of order 10^{-6} . By comparison when the baryonic power spectra are fitted to the SDSS DR7 power spectra data, larger values of α are allowed and the upper limit at 95% C. L. is 1.07×10^{-4} . This is because the dark matter power spectra are damped on small scales more quickly than the baryonic power spectra as shown in Fig. 7. From the thick lines in the left panel of Fig. 5, it is seen that the low-multipole CMB power spectrum for the barotropic model is obviously enhanced with the increasing α through the ISW effect. By using the data of CMB+SNIa+gISW, we obtain $\alpha < 3.97 \times 10^{-5}$ at the 95% C. L.

D. Geodesic model constraints

For the geodesic model, the constraints from the combination of various data are listed in Table II. The marginal 1D distributions and 2D contour plots from CMB+SNIa+BAO, CMB+SNIa+LSS(m), and CMB+SNIa+gISW are shown in Fig. 10.

CMB+SNIa+LSS(m) constraints allow negative mean value for α . Compared with results from CMB+SNIa+BAO and CMB+SNIa+LSS(m) constraints, CMB+SNIa+gISW gives a relatively narrow allowed range for α . The allowed range of the parameter α at the 95% C. L. in this case are $-0.16 < \alpha < 0.30$ from CMB+SNIa+BAO, $-0.20 < \alpha < 0.21$ from CMB+SNIa+LSS(m) and $-0.15 < \alpha < 0.26$ from CMB+SNIa+gISW, respectively. By comparison with the results for the barotropic model on the basis of the same data sets, the allowed region of parameter α for the geodesic model is obviously enlarged.

Parameters	CMB+SNIa+BAO	CMB+SNIa+LSS(m)	CMB+SNIa+gISW	CMB+SNIa+LSS(b)
$\Omega_b h^2$	$0.0225^{+0.0005}_{-0.0005}$	$0.0224^{+0.0005}_{-0.0005}$	$0.0224^{+0.0005}_{-0.0005}$	$0.0224^{+0.0005}_{-0.0005}$
$\Omega_{dm} h^2$	$0.1115^{+0.0033}_{-0.0032}$	$0.1156^{+0.0035}_{-0.0035}$	$0.1102^{+0.0038}_{-0.0038}$	$0.1156^{+0.0035}_{-0.0034}$
Θ_S	$1.0396^{+0.0025}_{-0.0025}$	$1.0396^{+0.0025}_{-0.0025}$	$1.0395^{+0.0025}_{-0.0025}$	$1.0395^{+0.0025}_{-0.0025}$
τ	$0.0872^{+0.0060}_{-0.0067}$	$0.0851^{+0.0062}_{-0.0072}$	$0.0880^{+0.0064}_{-0.0070}$	$0.0855^{+0.0061}_{-0.0066}$
α	$< 2.68 \times 10^{-3}$	$< 5.66 \times 10^{-6}$	$< 3.97 \times 10^{-5}$	$< 1.07 \times 10^{-4}$
n_s	$0.970^{+0.013}_{-0.012}$	$0.964^{+0.012}_{-0.012}$	$0.967^{+0.012}_{-0.012}$	$0.964^{+0.012}_{-0.012}$
$\log[10^{10} A_s]$	$3.081^{+0.033}_{-0.033}$	$3.090^{+0.032}_{-0.032}$	$3.075^{+0.034}_{-0.034}$	$3.091^{+0.032}_{-0.032}$
Ω_V	$0.73^{+0.01}_{-0.01}$	$0.71^{+0.02}_{-0.02}$	$0.74^{+0.02}_{-0.02}$	$0.71^{+0.02}_{-0.02}$
H_0	$70.8^{+1.3}_{-1.2}$	$69.1^{+1.5}_{-1.5}$	$71.2^{+1.5}_{-1.6}$	$69.1^{+1.5}_{-1.5}$

TABLE I: The mean values with 1σ errors and marginalized 95% C. L. of parameter α for the barotropic model using different combinations of data sets.

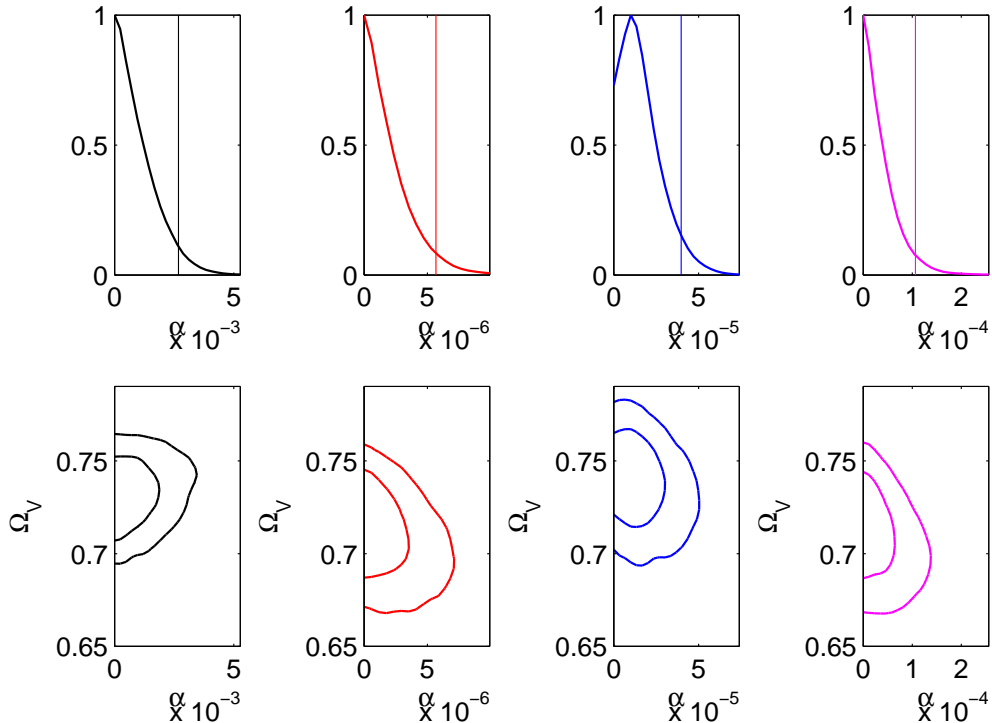


FIG. 9: The 1D marginalized distributions for the parameter α and 2D contours with 68% C. L. and 95% C. L. for the barotropic model using the combinations of data (left to right): CMB+BAO+SNIa (black line), CMB+SNIa+LSS(m) (red line), CMB+SNIa+gISW (blue line) and CMB+SNIa+LSS(b) (magenta line), respectively. The vertical lines in the top panels are the 95% confident levels.

Finally, in Fig. 11 we show gISW cross-correlation power spectra predicted by using the mean values of CMB+SNIa+gISW for the two models.

V. CONCLUSIONS

Any unified dark matter model can be decomposed into dark matter interacting with vacuum energy [34–36]. In such a decomposed model, the vacuum energy is coupled to dark matter and the energy-momentum transfer between the vacuum energy and the dark matter is given by the gradient of vacuum energy. Different covariant forms for the energy-momentum transfer four-vector have different effects on the CMB angular power spectrum and LSS power spectrum through the different evolution of inhomogeneous perturbation evolutions, even if the background cosmology is the same. Observational constraints on these decomposed models correspond to constraints on the interaction between dark matter and the vacuum energy, where we recover Λ CDM in the limit of zero interaction.

In this paper, we studied the evolution of perturbations in a decomposed Chaplygin gas model and compared

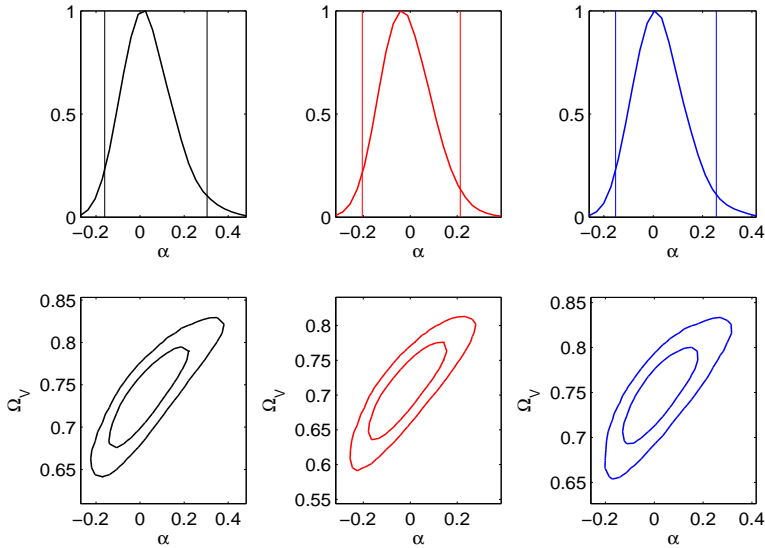


FIG. 10: The 1D marginalized distributions for the parameter α and 2D contours with 68% C. L. and 95% C. L. for the geodesic model using the combinations of data (left to right): CMB+SNIa+BAO (black line), CMB+SNIa+LSS(m) (red line), and CMB+SNIa+gISW (blue line), respectively. The vertical lines in the top panels are the 95% confident levels.

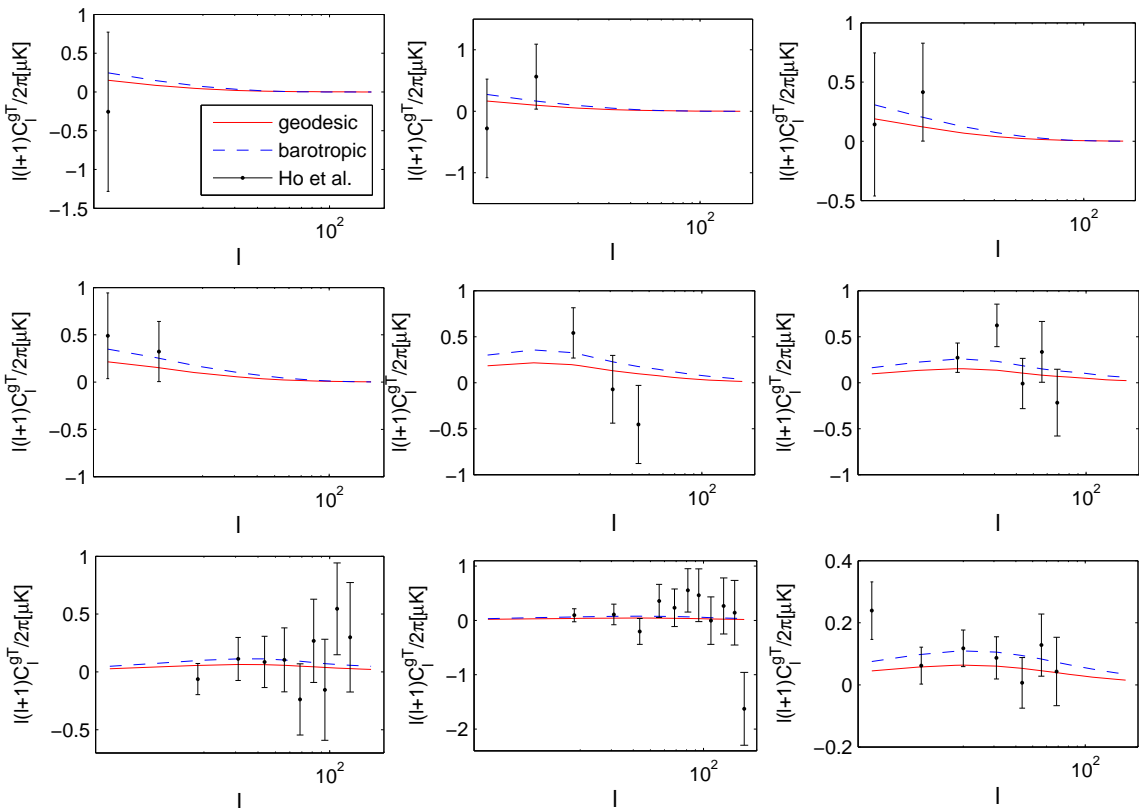


FIG. 11: The gISW cross-correlation power spectra with different galaxy samples for the barotropic model (dashed line) with mean values taken from CMB+SNIa+gISW constraints in the Table I and the geodesic model (solid line) with mean values taken from CMB+SNIa+gISW constraints in the Table II, respectively. The dots with error bars denote the gISW data from Ho et al. [41].

Parameters	CMB+SNIa+BAO	CMB+SNIa+LSS(m)	CMB+SNIa+gISW
$\Omega_b h^2$	$0.0224^{+0.0005}_{-0.0005}$	$0.0224^{+0.0005}_{-0.0005}$	$0.0225^{+0.0005}_{-0.0005}$
$\Omega_{dm} h^2$	$0.1077^{+0.0144}_{-0.0146}$	$0.1167^{+0.0149}_{-0.0150}$	$0.1062^{+0.0135}_{-0.0135}$
Θ_S	$1.0395^{+0.0026}_{-0.0026}$	$1.0394^{+0.0026}_{-0.0026}$	$1.0397^{+0.0025}_{-0.0025}$
τ	$0.0864^{+0.0063}_{-0.0072}$	$0.0862^{+0.0063}_{-0.0072}$	$0.0895^{+0.0065}_{-0.0076}$
α	$0.04^{+0.11}_{-0.11}$	$-0.01^{+0.11}_{-0.11}$	$0.03^{+0.10}_{-0.10}$
n_s	$0.964^{+0.013}_{-0.013}$	$0.965^{+0.013}_{-0.013}$	$0.967^{+0.013}_{-0.013}$
$\log[10^{10} A_s]$	$3.081^{+0.033}_{-0.033}$	$3.086^{+0.033}_{-0.033}$	$3.076^{+0.034}_{-0.034}$
Ω_V	$0.74^{+0.04}_{-0.04}$	$0.71^{+0.04}_{-0.04}$	$0.75^{+0.03}_{-0.03}$
H_0	$70.6^{+1.5}_{-1.5}$	$69.3^{+1.9}_{-1.9}$	$71.8^{+1.7}_{-1.7}$

TABLE II: The mean values with 1σ errors for the geodesic model using different combinations of data sets.

this with the evolution in a unified Chaplygin gas model with adiabatic perturbations. We considered two different models for the energy-momentum transfer in the decomposed case. In one model the energy-momentum transfer is along the gradient of the local dark matter density, in which case we recover the evolution equations for perturbations of a single barotropic fluid with the same equation of state as the generalised Chaplygin gas. The pressure perturbations are adiabatic and the rest-frame sound speed equals the adiabatic sound speed. This nonzero sound speed has an effect on both the CMB power spectrum and the LSS power spectrum. Increasing α enhances the CMB power spectra at the low multipoles. In addition, the effect on the total matter (baryon+dark matter) power spectrum caused by the sound speed is that there are decaying oscillations in the matter power spectrum for positive α , as for the generalised Chaplygin gas [21].

A different possibility which we considered is that the energy-momentum transfer is along the dark matter four-velocity, which leads to the dark matter following geodesics. Compared with the barotropic model, the geodesic model has a relative entropy perturbation between dark matter and vacuum energy. Thus the sound speed of the interacting dark matter+vacuum energy in the dark matter rest frame is zero. There are no oscillations or instabilities in the total matter power spectrum for positive or negative α .

In the decomposed Chaplygin gas, different interaction models can lead to very different evolutions of perturbations due to the different sound speeds. We test whether these two kinds of decomposed models can be supported or distinguished by current observations. We have constrained the barotropic model and geodesic model by using various combinations of data sets, including CMB constraints, type Ia supernovae, BAO distance measurements, large-scale structure and the integrated Sachs-Wolfe effect.

For the barotropic model the most stringent constraint on the α parameter is of the order of 10^{-6} from the combinations of CMB+SNIa+LSS(m), where the theoretical total matter (baryon+dark matter) power spectrum is fitted to the LSS power spectrum data. We conclude that a barotropic model must be extremely close to the Λ CDM model. In contrast the allowed region for the α parameter in the geodesic model is much larger, and negative α can also be compatible with the observations. The geodesic model thus allows significant deviations from the Λ CDM model.

In the case of a unified dark matter model it is not clear whether the galaxy power spectrum on large scales should follow the total matter power spectrum, which gives rise to the gravitaitonal potential, or the baryonic matter power spectrum, since only baryons follow geodesics. This choice leads to different predictions for the LSS power spectrum [23]. The same ambiguity applies in our barotropic model of interacting vacuum+dark matter, since the dark matter does not follow geodesics in this case, so we present constraints using LSS fitted to both the total matter power spectrum and the baryonic matter power spectrum. In the geodesic model, however, we only use the total matter power spectrum to fit the LSS power spectrum since both the dark matter and the baryons follow geodesics in this case and we expect the total matter overdensity to be responsible for the formation of collapsed halos. Nonetheless it would be interesting to study further the process of nonlinear collapse in this model and we hope to return to this question in future work.

Acknowledgments

Y. W. would like to thank Timothy Clemson, Lucas Lombriser, Gong-Bo Zhao for help with the CosmoMC and ISWWLL code. D. W. is supported by STFC Grant No. ST/H002774/1. L. X. is supported in part by NSFC under the Grants No. 11275035 and “the Fundamental Research Funds for the Central Universities” under the Grants No. DUT13LK01. J. D.-S. is supported by CONACYT Grant 210405. A. H. is supported by World Class University Grant No. R32-2009-000-10130-0 through the National Research Foundation, Ministry of Education, Science and Technology of Korea. All the numerical computations were done on the Sciamia High Performance Compute cluster, supported by the ICG SEPNet and University of Portsmouth. Y. W. and

J. D.-S. thank the ICG, University of Portsmouth for their hospitality.

- [1] M. Makler, S. Q. de Oliveira and I. Waga, Phys. Lett. B **555**, 1 (2003) [astro-ph/0209486].
- [2] A. Y. Kamenshchik, U. Moschella and V. Pasquier, Phys. Lett. B **511**, 265 (2001) [gr-qc/0103004];
- [3] M. C. Bento, O. Bertolami and A. A. Sen, Phys. Rev. D **66**, 043507 (2002) [gr-qc/0202064].
- [4] N. Bilic, G. B. Tupper and R. D. Viollier, Phys. Lett. B **535**, 17 (2002) [astro-ph/0111325].
- [5] M. Biesiada, W. Godlowski and M. Szydlowski, Astrophys. J. **622**, 28 (2005) [astro-ph/0403305].
- [6] R. Colistete and J. C. Fabris, Class. Quant. Grav. **22**, 2813 (2005) [astro-ph/0501519].
- [7] M. C. Bento, O. Bertolami, M. J. Reboucas and P. T. Silva, Phys. Rev. D **73**, 043504 (2006) [gr-qc/0512158].
- [8] M. C. Bento, O. Bertolami and A. A. Sen, Phys. Rev. D **67**, 063003 (2003) [astro-ph/0210468].
- [9] M. C. Bento, O. Bertolami and A. A. Sen, Phys. Lett. B **575**, 172 (2003) [astro-ph/0303538].
- [10] M. C. Bento, O. Bertolami and A. A. Sen, Gen. Rel. Grav. **35**, 2063 (2003) [gr-qc/0305086].
- [11] Z. H. Zhu, Astron. Astrophys. **423**, 421 (2004) [astro-ph/0411039].
- [12] P. Wu and H. Yu, Phys. Lett. B **644**, 16 (2007) [gr-qc/0612055].
- [13] J. C. Fabris, P. L. C. de Oliveira and H. E. S. Velten, arXiv:1106.0645 [astro-ph.CO].
- [14] Z. Li, P. Wu and H. Yu, JCAP **09**, 017 (2009) [arXiv:0908.3415[astro-ph.CO]].
- [15] O. Bertolami and P. T. Silva, astro-ph/0601507.
- [16] J. V. Cunha, J. S. Alcaniz and J. A. S. Lima, Phys. Rev. D **69**, 083501 (2004) [astro-ph/0306319];
J. S. Alcaniz and J. A. S. Lima, Astrophys. J. **618**, 16 (2005) [astro-ph/0308465].
Y. Gong, JCAP **0503**, 007 (2005) [astro-ph/0411253].
P. Wu and H. Yu, JCAP **0703**, 015 (2007) [astro-ph/0701446].
J. Lu, Y. Gui and L. Xu, Eur. Phys. J. C **63**, 349 (2009) [arXiv:1004.3365[astro-ph.CO]].
L. Xu and J. Lu, JCAP **1003**, 025 (2010) [arXiv:1004.3344[astro-ph.CO]].
N. Liang, L. Xu and Z. H. Zhu, Astronomy & Astrophysics, **527**, A11 (2011) [arXiv:1009.6059[astro-ph.CO]].
- [17] R. K. Sachs and A. M. Wolfe, Astrophys. J. **147**, 73 (1967).
- [18] D. Carturan and F. Finelli, Phys. Rev. D **68**, 103501 (2003) [astro-ph/0211626].
- [19] L. Amendola, F. Finelli, C. Burigana and D. Carturan, JCAP **0307**, 005 (2003) [astro-ph/0304325].
- [20] L. Xu, J. Lu and Y. Wang, Eur. Phys. J. C **72**, 1883 (2012) [arXiv:1204.4798].
- [21] H. Sandvik, M. Tegmark, M. Zaldarriaga and I. Waga, Phys. Rev. D **69**, 123524 (2004) [astro-ph/0212114].
- [22] M. Colless *et al.*, Mon. Not. Roy. Astron. Soc. **328**, 1039 (2001) [astro-ph/0106498v3];
M. Tegmark, A. J. S. Hamilton and Y. Xu, Mon. Not. Roy. Astron. Soc. **335**, 887 (2002) [astro-ph/0111575].
- [23] C. -G. Park, J. -c. Hwang, J. Park and H. Noh, Phys. Rev. D **81**, 063532 (2010) [arXiv:0910.4202 [astro-ph.CO]].
- [24] V. Gorini, A. Y. Kamenshchik, U. Moschella, O. F. Piattella and A. A. Starobinsky, J. Cosmol. Astropart. Phys. **02**, 016 (2008) [arXiv:0711.4242 [astro-ph]].
- [25] O. F. Piattella, D. Bertacca, M. Bruni and D. Pietrobon, JCAP **1001**, 014 (2010) [arXiv:0911.2664 [astro-ph.CO]].
- [26] D. Bertacca, M. Bruni, O. F. Piattella and D. Pietrobon, JCAP **1102**, 018 (2011) [arXiv:1011.6669 [astro-ph.CO]].
- [27] M. Bruni, R. Lazkoz and A. Rozas-Fernandez, arXiv:1210.1880 [astro-ph.CO].
- [28] R. R. R. Reis, I. Waga, M. O. Calvao and S. E. Joras Phys. Rev. D **68**, 061302 (2003) [astro-ph/0306004].
- [29] L. Amendola, I. Waga and F. Finelli, JCAP **0511**, 009 (2005) [astro-ph/0509099].
- [30] E. Gaztañaga, M. Manera and T. Multamaki, Mon. Not. Roy. Astron. Soc. **365**, 171 (2006) [astro-ph/0407022].
- [31] T. Giannantonio and A. Melchiorri, Class. Quant. Grav. **23**, 4125 (2006) [gr-qc/0606030].
- [32] W. Zimdahl and J. C. Fabris Class. Quant. Grav. **22**, 4311 (2005) [gr-qc/0504088].
- [33] L. P. Chimento, Phys. Rev. D **81**, 043525 (2010) [arXiv:0911.5687 [astro-ph.CO]].
- [34] M. C. Bento, O. Bertolami and A. A. Sen, Phys. Rev. D **70**, 083519 (2004) [astro-ph/0407239].
- [35] D. Wands, J. De-Santiago and Y. Wang, Class. Quant. Grav. **29**, 145017 (2012) [arXiv:1203.6776 [astro-ph.CO]].
- [36] J. De-Santiago, D. Wands and Y. Wang, arXiv:1209.0563 [astro-ph.CO].
- [37] E. Komatsu *et al.*, Astrophys. J. Suppl. **192**, 18 (2011) [arXiv:1001.4538[astro-ph.CO]];
<http://lambda.gsfc.nasa.gov/product/map/current/>.
- [38] N. Suzuki *et al.*, ApJ, **746**, 85 (2012) [arXiv:1105.3470[astro-ph.CO]].
- [39] W. J. Percival *et al.*, Mon. Not. Roy. Astron. Soc. **401**, 2148 (2010) [arXiv:0907.1660[astro-ph.CO]].
- [40] B. A. Reid *et al.*, Mon. Not. Roy. Astron. Soc. **404**, 60 (2010) [arXiv:0907.1659[astro-ph.CO]].
- [41] S. Ho, C. Hirata, N. Padmanabhan, U. Seljak and N. Bahcall, Phys. Rev. D. **78**, 043519 (2008) [arXiv:0801.0642].
- [42] V. F. Mukhanov, H. A. Feldman and R. H. Brandenberger, Phys. Rept. **215**, 203-333 (1992).
- [43] K. A. Malik, astro-ph/0101563.
- [44] K. A. Malik and D. Wands, Phys. Rept. **475**, 1 (2009) [arXiv:0809.4944[astro-ph.CO]].
- [45] K. A. Malik and D. Wands, JCAP **0502**, 007 (2005) [astro-ph/0411703].
- [46] H. Kodama and M. Sasaki, Prog. Theor. Phys. Suppl. **78**, 1 (1984).
- [47] K. A. Malik, D. Wands and C. Ungarelli, Phys. Rev. D **67**, 063516 (2003) [astro-ph/0211602].
- [48] <http://camb.info/>.
- [49] C. P. Ma and E. Bertschinger, Astrophys. J. **455**, 7 (1995) [astro-ph/9506072].
- [50] R. Bean and O. Doré, Phys. Rev. D **68**, 023515 (2003) [astro-ph/0301308].
- [51] R. Bean, E. E. Flanagan, I. Laszlo and M. Trodden, Phys. Rev. D **78**, 123514 (2008) [arXiv:0808.1105[astro-ph.CO]].
J. Q. Xia, Phys. Rev. D **80**, 103514 (2009) [arXiv:0911.4820[astro-ph.CO]].
- [52] J. Valiviita, E. Majorotto and R. Maartens, JCAP **0807**, 020 (2008) [arXiv:0804.0232[astro-ph.CO]].
- [53] K. Koyama, R. Maartens and Y. S. Song, JCAP **0910**, 017 (2009) [arXiv:0907.2126[astro-ph.CO]].
- [54] T. Koivisto, H. Kurki-Suonio, F. Ravndal Phys. Rev. D **71**, 064027 (2005) [astro-ph/0409163].

- [55] A. Lewis and S. Bridle, Phys. Rev. D **66**, 103511 (2002) [astro-ph/0205436].
- [56] <http://cosmologist.info/cosmomc/>.
- [57] S. Burles, K. M. Nollett and M. S. Turner, Astrophys. J. **552**, L1 (2001).
- [58] A. G. Riess *et al.*, ApJ, **730**, 119 (2011) [arXiv:1103.2976[astro-ph.CO]].
- [59] J. Dossett, M. Ishak and J. Moldenhauer, Phys. Rev. D **84**, 123001 (2011) [arXiv:1109.4583[astro-ph.CO]]; J. Dossett and M. Ishak, Phys. Rev. D **86**, 103008 (2012) [arXiv:1205.2422[astro-ph.CO]].
- [60] S. Cole *et al.*, Mon. Not. Roy. Astron. Soc. **362**, 505 (2005) [astro-ph/0501174].
- [61] N. Padmanabhan *et al.*, Mon. Not. Roy. Astron. Soc. **359**, 237 (2005) [astro-ph/0407594].